

Article

Commanded Filter-Based Robust Model Reference Adaptive Control for Quadrotor UAV with State Estimation Subject to Disturbances

Nigar Ahmed¹ and Nashmi Alrasheedi^{2,*} 

¹ College of Marine Electrical Engineering, Dalian Maritime University, Dalian 116062, China; nigar.ahmed.pk@gmail.com

² Department of Mechanical Engineering, College of Engineering, Imam Mohammad Ibn Saud Islamic University (IMSIU), Riyadh 11432, Saudi Arabia

* Correspondence: nhrasheedi@imamu.edu.sa

Abstract: Unmanned aerial vehicles must achieve precise flight maneuvers despite disturbances, parametric uncertainties, modeling inaccuracies, and limitations in onboard sensor information. This paper presents a robust adaptive control for trajectory tracking under nonlinear disturbances. Firstly, parametric and modeling uncertainties are addressed using model reference adaptive control principles to ensure that the dynamics of the aerial vehicle closely follow a reference model. To address the effects of disturbances, a modified nonlinear disturbance observer is designed based on estimated state variables. This observer effectively attenuates constant, nonlinear disturbances with variable frequency and magnitude, and noises. In the next step, a two-stage sliding mode control strategy is introduced, incorporating adaptive laws and a commanded-filter to compute numerical derivatives of the state variables required for control design. An error compensator is integrated into the framework to reduce numerical and computational delays. To address sensor inaccuracies and potential failures, a high-gain observer-based state estimation technique is employed, utilizing the separation principle to incorporate estimated state variables into the control design. Finally, Lyapunov-based stability analysis demonstrates that the system is uniformly ultimately bounded. Numerical simulations on a DJI F450 quadrotor validate the approach's effectiveness in achieving robust trajectory tracking under disturbances.

Keywords: aggressive trajectory tracking; adaptive control; disturbance observer; state observer; commanded filter; UAVs



Academic Editor: Mingjun Wei

Received: 1 February 2025

Revised: 26 February 2025

Accepted: 26 February 2025

Published: 28 February 2025

Citation: Ahmed, N.; Alrasheedi, N. Commanded Filter-Based Robust Model Reference Adaptive Control for Quadrotor UAV with State Estimation Subject to Disturbances. *Drones* 2025, 9, 181. <https://doi.org/10.3390/drones9030181>

Copyright: © 2025 by the authors. Licensee MDPI, Basel, Switzerland. This article is an open access article distributed under the terms and conditions of the Creative Commons Attribution (CC BY) license (<https://creativecommons.org/licenses/by/4.0/>).

1. Introduction

Unmanned aerial vehicles (UAVs) are flying robots that can be controlled autonomously or semi-autonomously from a ground station. Recent technological advancements have driven a significant rise in the use of UAVs across a wide range of applications, including military, remote sensing, wind turbine crack detection, commercial, and industrial domains. Due to their versatility, high maneuverability, lightweight design, cost-effectiveness, and vertical takeoff and landing (VTOL) capabilities, quadrotor UAVs have emerged as a prominent platform for various applications [1–5].

The propulsion system of a quadrotor UAV consists of four rotors mounted equidistantly from the center of gravity in the body frame, as illustrated in Figure 1. Quadrotors are inherently underactuated systems, with four control inputs and six outputs, including

attitude angles and Cartesian positions. Significant research efforts have been dedicated to the control design of quadrotor UAVs. However, the growing demand for innovative and dynamic applications has introduced new challenges in control system development. Moreover, the highly nonlinear and complex dynamics of quadrotors, coupled with disturbances, modeling and parametric uncertainties, actuator inefficiencies, sensor noise, and the need for aggressive maneuvers, make achieving effective trajectory tracking control a formidable task [6,7].

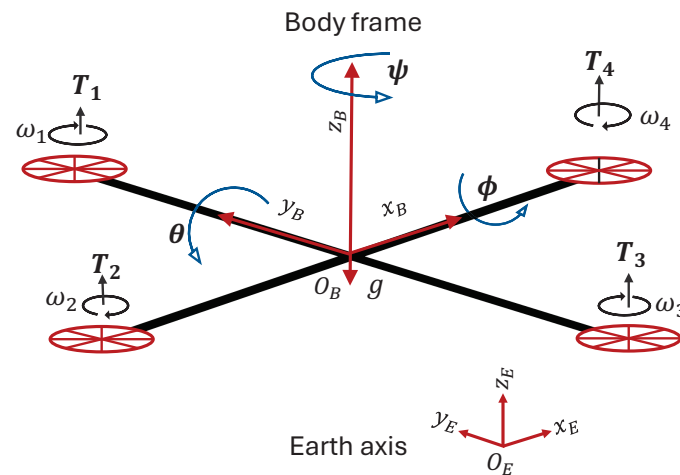


Figure 1. Quadrotor schematic.

Standard controllers based on linear and nonlinear control algorithms have been extensively utilized for quadrotor control. Linear control schemes typically require the model to be linearized, after which feedback control methods are employed to design controllers and achieve desired control objectives. Examples of such controllers include proportional–integral–derivative (PID) controllers [8], linear quadratic regulators (LQR) [9–11], and linearized model predictive control (MPC) [12–14]. However, linear control systems often neglect highly nonlinear dynamics, such as Coriolis terms, to meet the requirements of a linearized model. For instance, small attitude angles and slow linear or angular velocities are commonly assumed to be negligible.

To address the limitations and challenges associated with linear controllers, nonlinear control strategies such as sliding mode control (SMC), backstepping control, nonlinear dynamic inversion, nonlinear PID, model reference adaptive control (MRAC), and fuzzy controllers have been developed for quadrotor UAVs. These techniques are designed to achieve superior performance compared to linear controllers. Moreover, the aforementioned approaches effectively handle the complex dynamics and nonlinear coupling inherent in quadrotor UAVs, thereby achieving robustness and improved trajectory tracking performance [15].

SMC is widely regarded for its inherent robustness against matched uncertainties and disturbances. However, it introduces chattering in the control input due to its switching control strategy [16–18]. Furthermore, its robustness is only guaranteed when the upper bound of unknown uncertainties and disturbances is known [19]. In [20], a two-step SMC technique combined with adaptive laws was designed using Lyapunov stability criteria for quadrotor control. By incorporating a noise filter and a saturation function, the approach addressed sensor noise and modeling uncertainties. In [21], an adaptive SMC technique was employed to tackle the input saturation problem. Additionally, the use of adaptive laws facilitated disturbance rejection and eliminated the need for the empirical tuning of control gains. However, the inherent chattering issue, which causes wear and tear in actuators, remains unresolved in these methods.

In [22], a high-order sliding manifold was constructed to design a robust SMC technique that achieves a chattering-free controller and ensures asymptotic stability. The approach was combined with a high-order sliding mode observer (HOSMO) and a deadzone-based method for adaptive laws to tackle unknown disturbances during low-altitude grasping applications. A similar control technique with finite-time stability was proposed in [23], where all states were estimated using HOSMO based on the quadrotor's translational and rotational outputs. In this method, HOSMO provided disturbance estimates, which were utilized in the controller to achieve simultaneous disturbance rejection and chattering attenuation. In [24], saturation was introduced in the control input to solve the chattering issue. However, due to saturation function, the robustness of the control system was compromised. Other notable control techniques employing high-order sliding mode methods for solving chattering are presented in [25–28]. However, the high-order observer techniques in these controllers were sensitive to noise, and state convergence was not explicitly considered. Moreover, the chattering issue was not completely resolved.

Backstepping control is well-known for its Lyapunov-based design, which enables the development of chattering-free control algorithms to address wear and tear in quadrotor actuators. Its recursive design methodology, along with the cancellation of indefinite cross-coupling and nonlinear terms, ensures stability at each step and facilitates global stability [29–31]. Using the backstepping control technique, lateral position and altitude tracking performance were achieved in [32]. In this work, position and attitude tracking errors were first defined, and the Lyapunov method was applied to ensure negative semi-definiteness by canceling unwanted terms. In [33], backstepping control was combined with a correction term derived from the super-twisting algorithm to ensure disturbance attenuation and finite-time global stability of the origin. However, the recursive nature of backstepping control requires higher control effort due to cross-cancellation. Additionally, backstepping algorithms are susceptible to the '*explosion of complexity*' phenomenon caused by the repeated differentiation of virtual inputs and state variables [34].

Based on the first-order differentiator, the dynamic surface control (DSC) technique has been incorporated into the backstepping design procedure to address the issue of the repeated differentiation of virtual inputs, as presented in [35,36]. Additionally, adaptive control laws have been introduced to avoid the conservative tuning of control gains while ensuring the desired quadrotor performance. In [37], a commanded filter using Levant's differentiator was employed to compute numerical derivatives of the state variables and virtual control inputs. In this approach, tracking errors were first defined between the quadrotor outputs and the desired trajectory, and a commanded filter with error compensation was integrated into the controller to replace the derivatives. The concept of the commanded filter was extended in [6], where it facilitated numerical differentiation and disturbance attenuation through adaptive laws, enabling trajectory tracking in uncertain environments. However, implementing adaptive laws requires an accurate quadrotor model. Furthermore, adaptive laws are sensitive to noise and disturbances, which can lead to inaccuracies or instability in quadrotor performance [38].

Using an ideal quadrotor model, the model reference adaptive control (MRAC) technique has been employed for quadrotor attitude control, as demonstrated in [39]. In this method, an ideal reference attitude model was first designed, and an error was defined between the reference model and the actual quadrotor model. Adaptive laws were then formulated to satisfy matching conditions, followed by the design of a robust SMC-based control law. In similar research, quadrotor attitude stabilization was achieved in [40], but these techniques were limited to fully-actuated quadrotor attitude systems.

In [41], an MRAC-based trajectory tracking control strategy was proposed, achieving uniformly ultimately bounded (UUB) stability, and successfully validated through flight

tests on quadrotor systems. The self-regulation criteria in this technique ensured robustness against sensor noise and external disturbances. Although actuator dynamics were not explicitly considered, accurate quadrotor position and attitude measurements were essential for controller implementation. In [42], neural networks were incorporated into the MRAC framework to achieve disturbance attenuation and trajectory tracking for quadrotors with parametric uncertainties. However, the closed-loop system only demonstrated asymptotic convergence. Additionally, inevitable external disturbances, such as wind gusts, were neglected. Furthermore, selecting a suitable reference model remains a significant challenge, as the real quadrotor must accurately track the output of the reference model.

To address unknown disturbances, disturbance observers (DOs) have been extensively studied for quadrotor UAVs. Combined with controllers, disturbance observer-based control (DOBC) aims to simultaneously attenuate disturbances and achieve desired control objectives [43,44]. For disturbances with slow-varying behavior, they are often approximated as constant, enabling the lumping of all disturbances and uncertainties into a single term with an upper bound. A DO can then be designed for estimation, as illustrated in [45]. However, real-time quadrotor flights are subjected to nonlinear disturbances without known bounds, posing a challenge for DO design.

Nonlinear DOs, combined with observer-based SMC, have been utilized to estimate and reject faults and external disturbances in [46]. In this approach, a sliding mode observer was used for state estimation, while control objectives were achieved via SMC. Furthermore, actuator faults were addressed through sliding mode estimation. However, the chattering issue remained unresolved. Using the reinforcement learning approach, the fault tolerance was enhanced in [47]. In [48], a chattering-free DOBC was developed using robust control combined with nonlinear DO to handle exogenous wind disturbances and parametric uncertainties. However, the DO required prior knowledge of the constant peak-to-peak magnitude and frequency of disturbances, making it unsuitable for real-time implementation. Moreover, significant steady-state errors were observed in numerical simulations. In [49], state estimation for the time-delayed measurements was designed. This technique addressed uncertainties while utilizing the state-estimations for control performance. Other notable research on DOBC for quadrotors is presented in [50–56].

Implementing DOBC requires an accurate mathematical model of the quadrotor system and precise state information. However, inefficient sensors and actuators make achieving an effective DOBC algorithm challenging. In [57], fuzzy logic was combined with robust SMC for helical trajectory tracking. Although SMC is robust to bounded matched disturbances, the emphasis was on utilizing state estimation for quadrotor outputs and disturbance rejection. In [58], the controller and DO were designed separately, but this decomposition required a fully actuated control input and the assumption of no parametric uncertainties in the quadrotor system. In [59], disturbances were treated as an extended state, and state estimation criteria were employed for disturbance rejection using quadrotor outputs only. However, treating disturbances as an extended state necessitated an accurate quadrotor model. And ensuring that disturbance estimation dynamics were significantly faster than the control algorithm was difficult due to the coupled dynamics of state extension.

In recent years, Kalman filters (KFs) and their extended versions have gained popularity for quadrotor state estimation. For example, in [60], a Kalman filter was designed using control composition, quadrotor outputs, and model linearization to estimate position and attitude. However, disturbances were lumped into a constant bounded term prior to estimation, which is inadequate for real-time quadrotor flights. Additionally, the filtering problem for uncertain nonlinear quadrotor systems was not addressed. In [61], the load variation problem was solved using KFs. This method used KFs to predict outputs, followed by extended state estimation for disturbances. Other key works on KF and EKF applications

include [62–64]. Although KFs are optimal in minimizing mean square error and deliver remarkable results, they require the system to be linear, the state-space model to be known, and the noise to follow a Gaussian distribution with zero mean [65]. Additionally, the covariance matrices of noise must be known beforehand [66].

The high-gain observer (HGO) technique utilizes quadrotor outputs and nonlinear models to estimate states and their rates. HGO offers fast convergence, nonlinearity, and robustness to measurement noise [67,68]. However, it has not been extensively applied to quadrotor trajectory tracking. In limited literature, such as [69], HGO-based DOBC was used for state and fault estimation in the position control of quadrotors. Feedback linearization and adaptive laws were also introduced for online gain tuning. In [70], the HGO technique was modified by incorporating a dynamical filter on quadrotor outputs instead of measured outputs, addressing delayed measurements. An adaptive HGO-based backstepping control law combined with DO was proposed in [71]. This method eliminated reliance on measurable outputs, using estimated states and rates throughout the control algorithm, and simultaneously achieved state and disturbance estimation. Although the HGO technique has demonstrated significant potential in state estimation and control for quadrotors, its application to trajectory tracking remains relatively unexplored.

In summary, despite significant advancements in control algorithms using HGO for quadrotor trajectory tracking, notable research gaps persist. Based on the extensive literature review, studies such as MRAC combined with SMC [41,72] and MRAC integrated with DO [73] represent promising developments. However, to the best of the authors' knowledge, the integration of MRAC with SMC in conjunction with HGO-based state estimation has not been explored. Furthermore, the use of commanded filters within the MRAC framework to achieve the numerical differentiation of state variables and virtual control inputs remains uninvestigated. To bridge these gaps and address the challenges associated with trajectory tracking control design, this work makes the following key contributions:

1. Different from [39–42,72], the MRAC technique is combined with adaptive SMC based on commanded-filter and nonlinear DO to handle the high dynamics and aggressive maneuvers of the quadrotor.
2. Unlike prior works [19,38,44,52], a novel algorithm for nonlinear DO is developed, capable of estimating exogenous disturbances, constant disturbances, nonlinear disturbances with unknown variable frequency and magnitude, Gaussian-distributed random disturbances, uniformly-distributed random disturbances, and band-limited white noise.
3. A commanded-filter with error compensation is designed to perform numerical differentiation without relying on direct differentiators, thus avoiding computational delays in the control systems.
4. Two types of adaptive laws are proposed for online control gain tuning. First, an adaptive law is developed for the MRAC technique based on the tracking error between the reference model and the real model. Second, adaptive laws are introduced for the SMC control law based on the tracking error between the desired trajectory and quadrotor outputs. This approach also addresses the inherent chattering issue in SMC by reducing it through adaptive laws.
5. By employing the separation principle, the quadrotor outputs and their rates are replaced with the estimated states obtained using a HGO.

2. Mathematical Model and Preliminaries

Table 1 represents the nomenclature of mathematical model and the physical parameters of the DJI-F450 quadrotor UAV. It is assumed that the airframe inertia for roll, pitch, and yaw may vary depending on the drone and its propulsion system.

Table 1. DJI-F450 quadrotor parameters [74].

Nomenclature	Representation		Unit
Position	$x(t), y(t), z(t)$		m
Attitude angles	$\phi(t), \theta(t), \psi(t)$		rad
Attitude control	$U_i(t)$	$i \in (\phi, \theta, \psi)$	Nm
Position control	$U_p(t)$		N
Position virtual control	$U_j(t)$	$j \in (x, y, z)$	N
Angular velocities	ω_k	$k \in (1, 2, 3, 4)$	rad/s
Parameter	Symbol	Value	Unit
Gravity	g	9.81	m/s ²
Mass	m	2	kg
Length	l	0.225	m
Thrust coefficient	b	9.86×10^{-6}	Ns ²
Drag coefficient	d	1.6×10^{-7}	Nms ²
Rotor inertia	J_r	2.8×10^{-6}	kgm ²
Airframe inertia of roll	I_x	0.0035	kgm ²
Airframe inertia of pitch	I_y	0.0035	kgm ²
Airframe inertia of yaw	I_z	0.0035	kgm ²

2.1. Mathematical Model

Define $\mathbf{p} = [x, y, z]^T$ and $\Theta = [\phi, \theta, \psi]^T$ to represent position and attitude quadrotor, respectively. The rotational and translational velocities by $\Omega = [p, q, r]^T$ and $v = [v_x, v_y, v_z]^T$, respectively. Thus, the quadrotor motion can be given by the following [2]:

$$\begin{aligned}
 \dot{\mathbf{p}} &= v; \\
 \dot{v} &= -gz_e + \frac{T}{m} \mathbf{R}z_e \\
 \dot{\mathbf{R}} &= \mathbf{R}S(\Omega) \\
 \mathbf{I}_f \dot{\Omega} &= -\Omega \times \mathbf{I}_f \Omega - G_a + \tau_a
 \end{aligned} \tag{1}$$

where z_e is the unit vector along the z-axis in the earth-fixed inertial frame, $S(\Omega)$ is a skew-symmetric matrix, and \mathbf{R} is the rotational matrix given as follows [2,47]:

$$\mathbf{R} = \begin{bmatrix} \cos \theta \cos \psi & \sin \theta \sin \psi \sin \phi - \sin \psi \cos \phi & \sin \theta \cos \psi \cos \phi + \sin \psi \sin \phi \\ \cos \theta \sin \psi & \sin \theta \sin \psi \sin \phi + \cos \psi \cos \phi & \sin \theta \sin \psi \cos \phi - \cos \psi \sin \phi \\ -\sin \theta & \cos \theta \sin \phi & \cos \theta \cos \phi \end{bmatrix} \tag{2}$$

$\tau_a = [\tau_1, \tau_2, \tau_3]^T$ is the vector of torques generated by the rotors, where:

$$\tau_1 = bl(\omega_4^2 - \omega_2^2), \quad \tau_2 = bl(\omega_3^2 - \omega_1^2), \quad \tau_3 = d(\omega_2^2 + \omega_4^2 - \omega_1^2 - \omega_3^2) \tag{3}$$

The four control inputs of the quadrotor, combined with the total thrust, are given as follows:

$$\begin{bmatrix} T \\ \tau_1 \\ \tau_2 \\ \tau_3 \end{bmatrix} = \begin{bmatrix} U_p \\ U_\phi \\ U_\theta \\ U_\psi \end{bmatrix} = \begin{bmatrix} b & b & b & b \\ 0 & -bl & 0 & bl \\ -bl & 0 & bl & 0 \\ -d & d & -d & d \end{bmatrix} \begin{bmatrix} \omega_1^2 \\ \omega_2^2 \\ \omega_3^2 \\ \omega_4^2 \end{bmatrix} \tag{4}$$

After mathematical derivation and simplification, the dynamical model of the quadrotor can be expressed as follows:

$$\begin{cases} \ddot{x} = (\cos \phi \sin \theta \cos \psi + \sin \phi \sin \psi) \frac{U_p}{m} \\ \ddot{y} = (\cos \phi \sin \theta \sin \psi - \sin \phi \cos \psi) \frac{U_p}{m} \\ \ddot{z} = (\cos \phi \cos \theta) \frac{U_p}{m} - g \end{cases} \tag{5}$$

$$\begin{cases} \ddot{\phi} = \dot{\theta} \dot{\psi} \frac{(I_y - I_z)}{I_x} + \dot{\theta} \Omega_r \frac{I_r}{I_x} + U_\phi \frac{l}{I_x} \\ \ddot{\theta} = \dot{\phi} \dot{\psi} \frac{(I_z - I_x)}{I_y} - \dot{\phi} \Omega_r \frac{I_r}{I_y} + U_\theta \frac{l}{I_y} \\ \ddot{\psi} = \dot{\phi} \dot{\theta} \frac{(I_x - I_y)}{I_z} + \frac{U_\psi}{I_z} \end{cases}$$

where $\Omega_r = \omega_1 - \omega_2 + \omega_3 - \omega_4$. Next, for the state-space model of the quadrotor UAV, define $\phi = x_1(t)$, $\dot{\phi} = x_2(t)$, $\theta = x_3(t)$, $\dot{\theta} = x_4(t)$, $\psi = x_5(t)$, $\dot{\psi} = x_6(t)$, $x = x_7(t)$, $\dot{x} = x_8(t)$, $y = x_9(t)$, $\dot{y} = x_{10}(t)$, $z = x_{11}(t)$ and $\dot{z} = x_{12}(t)$. Simplification yields

$$\begin{bmatrix} \dot{x}_1(t) \\ \dot{x}_2(t) \\ \dot{x}_3(t) \\ \dot{x}_4(t) \\ \dot{x}_5(t) \\ \dot{x}_6(t) \\ \dot{x}_7(t) \\ \dot{x}_8(t) \\ \dot{x}_9(t) \\ \dot{x}_{10}(t) \\ \dot{x}_{11}(t) \\ \dot{x}_{12}(t) \end{bmatrix} = \begin{bmatrix} x_2(t) \\ a_\phi x_4(t)x_6(t) + b_\phi x_4(t)\Omega_r + c_\phi U_\phi(t) \\ x_4(t) \\ a_\theta x_2(t)x_6(t) - b_\theta x_2(t)\Omega_r + c_\theta U_\theta(t) \\ x_6(t) \\ a_\psi x_2(t)x_4(t) + c_\psi U_\psi(t) \\ x_8(t) \\ \frac{1}{m} (\cos \phi(t) \sin \theta(t) \cos \psi(t) + \sin \phi(t) \sin \psi(t)) U_p(t) \\ x_{10}(t) \\ \frac{1}{m} (\cos \phi(t) \sin \theta(t) \sin \psi(t) - \sin \phi(t) \cos \psi(t)) U_p(t) \\ x_{12}(t) \\ \frac{1}{m} \cos x_1(t) \cos x_3(t) U_p(t) - g \end{bmatrix} \tag{6}$$

where $a_\phi = (I_y - I_z) / I_x$, $b_\phi = I_r / I_x$, $c_\phi = l / I_x$, $a_\theta = (I_z - I_x) / I_y$, $b_\theta = I_r / I_y$, $c_\theta = l / I_y$, $a_\psi = (I_x - I_y) / I_z$, $c_\psi = 1 / I_z$.

2.2. Lemmas and Assumptions

This section presents the key lemmas and underlying assumptions that serve as the foundation for the proposed control design methodology.

Lemma 1. According to [2,58], quadrotor dynamical model can be decoupled into attitude and position subsystems using small-angle approximation which states that $\theta \approx 0$ implies $\cos \theta \approx 1$ and $\sin \theta \approx 0$.

Lemma 2. According to [75], for a continuous function with a bounded initial condition, define $\forall t \in R^+$ and satisfy $V(t) \geq 0$; then, for positive constants a_1 and b_1 , the function $V(t)$ is uniformly ultimately bounded, if it can be deduced that $\dot{V}(t) \leq -a_1 V + b_1$.

Lemma 3. First order Levant differentiator for an input signal; v_r defined for the time interval $[0, \infty]$ is given by $\zeta_1 = v$; $\zeta_2 = -\kappa_2 \text{sign}(\zeta_1 - v_r)$, where κ_1 and κ_2 are positive design constants. $v = -\kappa_1 |\zeta_1 - v_r|^{\frac{1}{2}} \text{sign}(\zeta_1 - v_r) + \zeta_2$ [76].

Lemma 4. The error between differentiated signals using the Levant differentiator and real signal is bounded by a small constant, i.e., $|\zeta_1 - v_r| \leq \epsilon$, where $\epsilon > 0$ is a small constant [37].

Assumption 1. Roll and pitch angles stay within $(-\frac{\pi}{2}, \frac{\pi}{2})$ [2].

Assumption 2. The desired reference trajectory is continuous and bounded.

Assumption 3. *Quadrotor attitude and position are measurable.*

3. Control Design and Stability Analysis

3.1. Attitude Control

Without loss of generality, consider the decoupled roll model in the attitude state-space representation, subject to nonlinear disturbances. The controller is designed to achieve tracking control performance, and the state-space model is given as follows:

$$\begin{aligned} \dot{x}_1(t) &= x_2(t) \\ \dot{x}_2(t) &= a_\phi x_4(t)x_6(t) + b_\phi x_4(t)\Omega_r + c_\phi U_\phi(t) + d_\phi(t) \end{aligned} \quad (7)$$

where $d_\phi(t)$ represents the bounded nonlinear disturbance estimated using the technique given by $\hat{d}_\phi(t) = z_\phi(t) + w_\phi(t)$, where

$$\begin{aligned} \dot{z}_\phi(t) &= -\mu_\phi (a_\phi x_4(t)x_6(t) + b_\phi x_4(t)\Omega_r + c_\phi U_\phi(t) + w_\phi(t) + z_\phi(t)) \\ w_\phi(t) &= \mu_\phi x_2(t) \end{aligned} \quad (8)$$

where μ_ϕ denotes a positive DO control gain. Next, the error dynamics can be analysed by defining $\tilde{d}_\phi(t) = d_\phi(t) - \hat{d}_\phi(t)$. Thus, it can be derived that

$$\begin{aligned} \dot{\tilde{d}}_\phi &= \dot{d}_\phi(t) - \dot{\hat{d}}_\phi(t) \\ &= \dot{d}_\phi(t) - (-\mu_\phi (a_\phi x_4(t)x_6(t) + b_\phi x_4(t)\Omega_r + c_\phi U_\phi(t) + w_\phi(t) + z_\phi(t)) + \mu_\phi \dot{x}_2(t)) \\ &= \dot{d}_\phi(t) - (-\mu_\phi (a_\phi x_4(t)x_6(t) + b_\phi x_4(t)\Omega_r + c_\phi U_\phi(t) + w_\phi(t) + z_\phi(t)) \\ &\quad + \mu_\phi (a_\phi x_4(t)x_6(t) + b_\phi x_4(t)\Omega_r + c_\phi U_\phi(t) + d_\phi(t))) \\ &= \dot{d}_\phi(t) - \mu_\phi (d_\phi(t) - \hat{d}_\phi(t)) \end{aligned} \quad (9)$$

Introducing Young's inequality and simplify

$$\begin{aligned} \dot{\tilde{d}}_\phi(t) &\leq -\mu_\phi \tilde{d}_\phi(t) + \frac{1}{2} (1 + \tilde{d}_\phi^2) \\ &\leq -\mu_\phi \tilde{d}_\phi(t) + \frac{1}{2} \bar{d}_\phi \end{aligned} \quad (10)$$

where $\bar{d}_\phi \geq \max\{1 + \tilde{d}_\phi^2\}$ is a maximum bound. Since, $\bar{d}_\phi > 0 \forall t \geq 0$, therefore, with $\mu_\phi > 0$ sufficiently large, the nonlinear DO will converge and estimate the disturbance. Next, define

$$X_\phi = \begin{bmatrix} x_1(t) \\ x_2(t) \end{bmatrix}; F_\phi(t) = \begin{bmatrix} x_2(t) \\ f_\phi(t) \end{bmatrix}; B_\phi = \begin{bmatrix} 0 \\ c_\phi \end{bmatrix}; D_\phi = \begin{bmatrix} 0 \\ 1 \end{bmatrix} \quad (11)$$

where $f_\phi(t) = a_\phi x_4(t)x_6(t) + b_\phi x_4(t)\Omega_r$. Hence, it can be written that

$$\dot{X}_\phi = F_\phi(t) + B_\phi U_\phi + D_\phi d_\phi(t) \quad (12)$$

The MRAC control technique developed in this research requires the matching conditions to be satisfied between the real and reference models. Therefore, the roll model must be transformed into the desired model in matrix form. Based on this, the roll control input, $U_\phi(t)$, for feedback linearization is chosen as follows:

$$U_\phi(t) = \left(\frac{1}{B_\phi^T B_\phi} \right) B_\phi^T \{A_1 X_\phi - F_\phi(t) + B_1 v_\phi(t)\} \quad (13)$$

where v_ϕ is a virtual control input to be designed using the MRAC-SMC technique combined with nonlinear DO. $A_1 = \begin{bmatrix} 0 & 0; k_1 & k_2 \end{bmatrix}$ and $B_1 = \begin{bmatrix} 0 & k_3 \end{bmatrix}^T$, with $k_1 > 0, k_2 > 0$ and $k_3 > 0$.

Remark 1. A_1 and B_1 are selected to ensure that the state variables are explicitly represented in the linearized system following the introduction of feedback linearization, which is employed to eliminate nonlinear coupled terms.

Next, substitute (13) into (12)

$$\dot{X}_\phi = A_\phi X_\phi + B_\phi v_\phi + D_\phi d_\phi \quad (14)$$

where

$$A_\phi = \begin{bmatrix} 0 & 1 \\ k_1 & k_2 \end{bmatrix}; B_\phi = \begin{bmatrix} 0 \\ B_\phi \left(\frac{1}{B_\phi^T B_\phi} \right) B_\phi^T B_1 \end{bmatrix} \quad (15)$$

where $B_\phi \left(\frac{1}{B_\phi^T B_\phi} \right) B_\phi^T B_1 = k_3$. Now, the virtual control input for the design of adaptive laws using MRAC criteria is chosen as follows:

$$v_\phi(t) = \hat{K}_\phi(t) X_\phi + \hat{K}_{r_\phi}(t) r_\phi(t) - \hat{K}_{v_\phi}(t) \bar{u}_\phi(t) \quad (16)$$

where $r_\phi(t)$ is the reference input, and $\hat{K}_\phi(t)$, $\hat{K}_{r_\phi}(t)$, and $\hat{K}_{v_\phi}(t)$ are adaptive gains to be designed. $\bar{u}_\phi(t)$ is a chattering-free robust SMC for trajectory tracking. In next step, the reference model is chosen according to the second-order dynamical system, given as follows:

$$\ddot{x}_m + 2\zeta_m \omega_m \dot{x}_m + \omega_m^2 x_m = b_m r_\phi(t) \quad (17)$$

where x_m is the state variable of the reference model. ζ_m and ω_m are the damping ratio and natural frequency, respectively. They should be chosen such that the reference model satisfies the Hurwitz criteria. Furthermore, b_m is a constant and $r_\phi(t)$ is the known reference input. Simplification is given as follows:

$$\dot{X}_m = A_m X_m + B_m r_\phi(t); A_m = \begin{bmatrix} 0 & 1 \\ -\omega_m^2 & -2\zeta_m \omega_m \end{bmatrix}; B_m = \begin{bmatrix} 0 \\ b_m \end{bmatrix} \quad (18)$$

Error between real and reference model is defined as follows:

$$e_\phi = X_\phi - X_m \quad (19)$$

Time derivative is given by

$$\dot{e}_\phi = A_\phi X_\phi + B_\phi v_\phi + D_\phi d_\phi - A_m X_m - B_m r_\phi(t) \quad (20)$$

Substituting (16) into (19)

$$\begin{aligned} \dot{e}_\phi &= (A_\phi + B_\phi \hat{K}_\phi) X_\phi - A_m X_m + (B_\phi \hat{K}_{r_\phi}(t) - B_m) r_\phi(t) - B_\phi \hat{K}_{v_\phi}(t) \bar{u}_\phi(t) \\ &+ D_\phi d_\phi(t) \end{aligned} \quad (21)$$

Matching conditions for designing adaptive gains for MRAC technique should satisfy

$$\begin{aligned} A_\phi + B_\phi \hat{K}_\phi &= A_m \\ B_\phi \hat{K}_{r_\phi} &= B_m \end{aligned} \quad (22)$$

Next, (21) can be simplified as follows:

$$\begin{aligned} \dot{e}_\phi &= (A_\phi + B_\phi K_\phi) X_\phi - A_m X_m - B_\phi \tilde{K}_\phi X_\phi - B_\phi \tilde{K}_{r_\phi} r_\phi(t) - (B_\phi K_r - B_m) r_\phi(t) \\ &+ B_\phi \tilde{K}_{v_\phi}(t) \bar{u}_\phi(t) - B_\phi K_v \bar{u}_\phi(t) + D_\phi d_\phi(t) \end{aligned} \quad (23)$$

where

$$\tilde{K}_\phi = K_\phi - \hat{K}_\phi(t); \tilde{K}_{r_\phi}(t) = K_{r_\phi} - \hat{K}_{r_\phi}(t); \tilde{K}_{v_\phi}(t) = K_{v_\phi} - \hat{K}_{v_\phi}(t) \quad (24)$$

where K_ϕ , K_{r_ϕ} , and K_{v_ϕ} are unknown positive ideal gains. Hence, it can be derived that

$$\dot{e}_\phi = A_\phi e_\phi - B_\phi \tilde{K}_\phi X_\phi - B_\phi \tilde{K}_{r_\phi} r_\phi(t) + B_\phi \tilde{K}_{v_\phi} \bar{u}_\phi(t) - B_\phi K_{v_\phi} \bar{u}_\phi(t) + D_\phi d_\phi(t) \quad (25)$$

Next, the Lyapunov function is chosen as follows:

$$V_\phi = e_\phi^T P e_\phi + c_\phi \left(\tilde{K}_\phi \Gamma_\phi^{-1} \tilde{K}_\phi^T + \frac{1}{\alpha_\phi} \tilde{K}_{r_\phi}^2 + \frac{1}{\beta_\phi} \tilde{K}_{v_\phi}^2 \right) \quad (26)$$

where $P_\phi A_\phi + A_\phi^T P_\phi = -Q_\phi$, $P_\phi = P_\phi^T > 0$ and $Q_\phi = Q_\phi^T$. Furthermore, $\Gamma_\phi = \Gamma_\phi^T \in R^{2 \times 2}$, α_ϕ and β_ϕ are adaptive control tuning gains. Next, time derivative is derived as follows:

$$\dot{V}_\phi = \dot{e}_\phi^T P_\phi e_\phi + e_\phi^T P_\phi \dot{e}_\phi + c_\phi \left(2\tilde{K}_\phi \Gamma_\phi^{-1} \dot{\tilde{K}}_\phi + \frac{2}{\alpha_\phi} \tilde{K}_{r_\phi} \dot{\tilde{K}}_{r_\phi} + \frac{2}{\beta_\phi} \tilde{K}_{v_\phi} \dot{\tilde{K}}_{v_\phi} \right) \quad (27)$$

Substituting (25) into (27)

$$\begin{aligned} \dot{V}_\phi = & \left(e_\phi^T A_\phi^T - X_\phi^T \tilde{K}_\phi^T B_\phi^T - r_\phi(t) \tilde{K}_{r_\phi}^T B_\phi^T + \bar{u}_\phi(t) \tilde{K}_{v_\phi}^T B_\phi^T + d_\phi(t) D_\phi^T \right) P e_\phi \\ & + e_\phi^T P_\phi \left(A_\phi e_\phi - B_\phi \tilde{K}_\phi X_\phi - B_\phi \tilde{K}_{r_\phi} r_\phi(t) + B_\phi \tilde{K}_{v_\phi} \bar{u}_\phi(t) + D_\phi d_\phi(t) \right) \\ & + c_\phi \left(2\tilde{K}_\phi \Gamma_\phi^{-1} \dot{\tilde{K}}_\phi + \frac{2}{\alpha_\phi} \tilde{K}_{r_\phi} \dot{\tilde{K}}_{r_\phi} + \frac{2}{\beta_\phi} \tilde{K}_{v_\phi} \dot{\tilde{K}}_{v_\phi} \right) \end{aligned} \quad (28)$$

Simplifying

$$\begin{aligned} \dot{V}_\phi = & e_\phi^T (P_\phi A_\phi + A_\phi^T P_\phi) e_\phi + 2e_\phi^T P_\phi B_\phi (-\tilde{K}_\phi X_\phi - \tilde{K}_{r_\phi} r_\phi(t) + \tilde{K}_{v_\phi} \bar{u}_\phi(t) \\ & - K_{v_\phi} \bar{u}_\phi(t)) + 2e_\phi^T P_\phi D_\phi d_\phi(t) + c_\phi \left(2\tilde{K}_\phi \Gamma_\phi^{-1} \dot{\tilde{K}}_\phi + \frac{2}{\alpha_\phi} \tilde{K}_{r_\phi} \dot{\tilde{K}}_{r_\phi} + \frac{2}{\beta_\phi} \right. \\ & \left. \times \tilde{K}_{v_\phi} \dot{\tilde{K}}_{v_\phi} \right) \end{aligned} \quad (29)$$

Hence, it can be obtained

$$\begin{aligned} \dot{V}_\phi = & -e_\phi^T Q_\phi e_\phi + 2c_\phi \tilde{K}_\phi \left(\Gamma_\phi^{-1} \dot{\tilde{K}}_\phi^T - k_3 X_\phi e_\phi^T \bar{P}_2 \right) + 2c_\phi \tilde{K}_{r_\phi} \left(\frac{1}{\alpha_\phi} \dot{\tilde{K}}_{r_\phi} - k_{r_\phi} r_\phi(t) e_\phi^T \right. \\ & \left. \times \bar{P}_2 \right) + 2c_\phi \tilde{K}_{v_\phi} \left(\frac{1}{\beta_\phi} \dot{\tilde{K}}_{v_\phi} + k_3 \bar{u}_\phi(t) e_\phi^T \bar{P}_2 \right) - 2k_3 e_\phi^T \bar{P}_2 K_{v_\phi} \bar{u}_\phi(t) \\ & + 2e_\phi^T \bar{P}_2 d_\phi(t) \end{aligned} \quad (30)$$

where \bar{P}_2 is the second column of P_ϕ . Furthermore, $2e_\phi^T P_\phi B_\phi = 2k_3 e_\phi^T \bar{P}_2 \in R$ and $2e_\phi^T P_\phi D_\phi = 2e_\phi^T \bar{P}_2 \in R$. Choose adaptive laws as follows:

$$\dot{\tilde{K}}_\phi^T(t) = -\Gamma_\phi X_\phi e_\phi^T \bar{P}_2; \dot{\tilde{K}}_{r_\phi}(t) = -\alpha_\phi k_3 r_\phi(t) e_\phi^T \bar{P}_2; \dot{\tilde{K}}_{v_\phi}(t) = -\beta_\phi k_3 \bar{u}_\phi(t) e_\phi^T \bar{P}_2 \quad (31)$$

Substituting (31) into (30) yields

$$\begin{aligned} \dot{V}_\phi = & -e_\phi^T Q_\phi e_\phi - 2k_3 e_\phi^T \bar{P}_2 K_{v_\phi} \bar{u}_\phi(t) + 2e_\phi^T \bar{P}_2 d_\phi(t) \\ & \leq -e_\phi^T Q_\phi e_\phi + \gamma_\phi + \bar{b}_\phi \end{aligned} \quad (32)$$

where $\gamma_\phi = 2e_\phi^T \bar{P}_2 (k_3^2 + 1)$ is a known constant, and $\bar{b}_\phi \geq \frac{1}{2} \max\{\bar{u}_\phi^2(t) + d_\phi^2(t)\}$ represents an upper bound on the SMC input and disturbance. Therefore, the uniformly ultimately bounded condition can be achieved, provided that P_ϕ is appropriately designed.

It is important to note that since $d_\phi(t)$ is bounded, its square is also bounded. Furthermore, $\bar{u}_\phi(t)$ is a control input designed using SMC principles, which inherently ensures boundedness if the control gains are chosen to be positive. Consequently, its squared value is also bounded. The design of $\bar{u}_\phi(t)$ will be presented next after the model is redesigned as follows:

$$\dot{X}_\phi = A_\phi X_\phi + B_\phi \bar{u}_\phi + D_\phi d_\phi \tag{33}$$

Next, for the design of $\bar{u}_\phi(t)$, firstly the commanded-filter is introduced as $\dot{Z}_\phi = \mathbb{P}_\phi Z_\phi$, written as follows:

$$\begin{bmatrix} \dot{z}_1 \\ \dot{z}_2 \end{bmatrix} = \begin{bmatrix} -p_1 |z_1 - \phi_r|^{1/2} & 1 \\ -p_2 & 0 \end{bmatrix} \begin{bmatrix} \text{sign}(z_1 - \phi_r) \\ z_2 \end{bmatrix} \tag{34}$$

where ϕ_r is the desired roll angle to be differentiated. $p_1 > 0$ and $p_2 > 0$ are design constants. Furthermore, $z_1 = x^c$ and $z_2 = \dot{x}^c = \dot{\phi}_r$, represent the output of the commanded filter and the derivative of the input signal, respectively. To handle the numerical differentiation errors, a compensation system is designed as $\dot{\mathbb{E}}_\phi = \mathfrak{R}_\phi \mathbb{E}_\phi + \mathbb{X}_\phi$, written as follows:

$$\begin{bmatrix} \dot{\xi}_1(t) \\ \dot{\xi}_2(t) \end{bmatrix} = \begin{bmatrix} -r_1 & 1 \\ -1 & -r_2 \end{bmatrix} \begin{bmatrix} \xi_1 \\ \xi_2 \end{bmatrix} + \begin{bmatrix} (x^c(t) - \phi_r) \\ 0 \end{bmatrix} \tag{35}$$

where $r_1 > 0$ and $r_2 > 0$ are design constants. Next, the sliding manifold is chosen as follows:

$$S_\phi = C_\phi^T (X_\phi - Z_\phi - \mathbb{E}_\phi) \tag{36}$$

where $C_\phi = [c_1; 1]$, with $c_1 > 0$. Next, the sliding mode surface dynamics are obtained as follows:

$$\dot{S}_\phi = C_\phi^T (A_\phi X_\phi + B_\phi \bar{u}_\phi + D_\phi d_\phi - \mathbb{P}_\phi Z_\phi - \mathfrak{R}_\phi \mathbb{E}_\phi - \mathbb{X}_\phi) \tag{37}$$

Hence, the control input is chosen as follows:

$$\begin{aligned} \bar{u}_\phi = & - \left(C_\phi^T B_\phi \right)^{-1} \left(C_\phi^T \left(A_\phi X_\phi + D_\phi \hat{d}_\phi(t) - \mathbb{P}_\phi Z_\phi - \mathfrak{R}_\phi \mathbb{E}_\phi - \mathbb{X}_\phi \right) \right. \\ & \left. + \hat{L}_\phi \text{sgn}(S_\phi) + \hat{K}_\phi S_\phi \right) \end{aligned} \tag{38}$$

Since $\bar{u}_\phi \in R$, it can be written as follows:

$$\begin{aligned} \bar{u}_\phi = & - \frac{1}{k_3} \left(c_1 (x_2 + p_1 |z_1 - \phi_r|^{1/2} \text{sign}(z_1 - \phi_r) - x^c(t) + \phi_r) + k_1 x_1 + k_2 x_2 \right. \\ & + b_\phi x_4(t) \Omega_r + \hat{d}_\phi + (p_2 - c_1) z_2 + (r_1 + 1) \xi_1 + (r_2 - 1) \xi_2 + \hat{L}_\phi \text{sgn} S_\phi \\ & \left. + \hat{K}_\phi S_\phi \right) \end{aligned} \tag{39}$$

where adaptive laws are governed as follows:

$$\dot{\hat{L}}_\phi = \gamma_\phi |S_\phi|; \dot{\hat{K}}_\phi = \eta_\phi S_\phi^2 \text{ where } \hat{L}_\phi(0) = 0, \hat{K}_\phi(0) = 0 \tag{40}$$

where $\gamma_\phi > 0$ and $\eta_\phi > 0$ are control gains for adaptive laws.

Remark 2. $\hat{L}_\phi(t)$ and $\hat{K}_\phi(t)$ will be non-negative if the adaptive control gains satisfy $\gamma_\phi > 0$ and $\eta_\phi > 0$.

Next, define Lyapunov function as follows:

$$V_S = \frac{1}{2} S_\phi^2 + \frac{1}{2\gamma_\phi} \tilde{L}_\phi^2 + \frac{1}{2\eta_\phi} \tilde{K}_\phi^2 \tag{41}$$

where $\tilde{L}_\phi = L - \hat{L}_\phi$ and $\tilde{K}_\phi = K_\phi - \hat{K}_\phi$. Now, time derivative is obtained as

$$\dot{V}_S = S_\phi \dot{S}_\phi - \frac{1}{\gamma_\phi} \tilde{L}_\phi \dot{\tilde{L}}_\phi - \frac{1}{\eta_\phi} \tilde{K}_\phi \dot{\tilde{K}}_\phi \tag{42}$$

Next, by using (36) and (39), the time derivative can be obtained as follows:

$$\dot{V}_S \leq -L_\phi |S_\phi| - K_\phi S_\phi^2 + \tilde{L}_\phi \left(|S_\phi| - \frac{1}{\gamma_\phi} \dot{\tilde{L}}_\phi \right) + \tilde{K}_\phi \left(S_\phi^2 - \frac{1}{\eta_\phi} \dot{\tilde{K}}_\phi \right) \tag{43}$$

Introducing (40) yields

$$\dot{V}_S \leq -L_\phi |S_\phi| - K_\phi S_\phi^2 \tag{44}$$

Hence, the controller is stable if the adaptive control gains, i.e., γ_ϕ and η_ϕ , are designed positive and sufficiently large. Since $\hat{L}_\phi(t)$ and $\hat{K}_\phi(t)$ remain non-negative if the adaptive control gains satisfy $\gamma_\phi > 0$ and $\eta_\phi > 0$, the positivity of these terms is evident from the adaptive law design. This is because the right-hand side of both adaptive laws is always non-negative. However, it should be noted that these terms will not increase indefinitely over time, as the sliding mode surface eventually converges to zero, leading to a steady-state condition for the adaptive laws.

Consequently, $\hat{L}_\phi(t) \rightarrow L_\phi$ and $\hat{K}_\phi(t) \rightarrow K_\phi$, where L_ϕ and K_ϕ are unknown positive constants, and the adaptive law ensures a dynamic convergence to these values.

Next, for obtaining the estimated roll and its rate, following the HGO technique is designed $\dot{\hat{X}}_\phi = F_\phi(t) + B_\phi U_\phi + \mathbb{K}_\phi(y_\phi - \hat{x}_1)(t)$, where $y_\phi = x_1$ is the real output of the roll model and

$$\hat{X}_\phi = [\hat{x}_1 \quad \hat{x}_2]^T; F_\phi(t) = [x_8 \quad \hat{f}_1(t)]^T; B_\phi = [0 \quad 1]^T; \mathbb{K}_\phi = \frac{1}{\varepsilon^2} \begin{bmatrix} \varepsilon \hat{h}_{\phi 1} & 0 \\ 0 & \hat{h}_{\phi 2} \end{bmatrix} \tag{45}$$

where $\varepsilon = (0, 1]$, $\hat{h}_{\phi 1} > 0$ and $\hat{h}_{\phi 2} > 0$ are observer gains. $\hat{f}_1(t) = a_\phi \hat{x}_4(t) \hat{x}_6(t) + b_\phi \hat{x}_4(t) \Omega_r$.

Corollary 1 ([67]). *Design of sufficiently large state-observer gains results in the estimated-state trajectories recovering the performance of the real-state trajectories, such that $\tilde{f}_\phi = (f_\phi - \hat{f}_\phi) \rightarrow 0$ when $t \rightarrow \infty$.*

In order to analyse error dynamics, define estimation errors as follows:

$$\chi_1 = \frac{1}{\varepsilon} \tilde{x}_1; \chi_2 = \tilde{x}_2 \tag{46}$$

Let $\chi_\phi = [\chi_1, \chi_2]^T$; then, taking the derivative and simplifying yields $\varepsilon \dot{\chi}_\phi = \mathbb{A} \chi_\phi + \varepsilon \delta$, where matrices δ and \mathbb{A} are written as follows:

$$\mathbb{A} = \begin{bmatrix} -\hat{h}_{\phi 1} & 1 \\ -\hat{h}_{\phi 2} & 0 \end{bmatrix}; \delta = \begin{bmatrix} 0 \\ \tilde{f}_\phi \end{bmatrix} \tag{47}$$

where \mathbb{A} is Hurwitz due to the characteristic polynomial gains $\hat{h}_{\phi 1}$ and $\hat{h}_{\phi 2}$. Now, choose a Lyapunov candidate function as follows:

$$V_H = \chi_\phi^T \mathbb{P} \chi_\phi \tag{48}$$

where $\mathbb{P} = [p_{11}, p_{12}; p_{21}, p_{22}]$ with positive constants such that $\mathbb{P} = \mathbb{P}^T > 0$ and $p_{12} = p_{21}$. In addition, \mathbb{P} is obtained by solving $\mathbb{P}\mathbb{A} + \mathbb{A}^T\mathbb{P} = -\mathbb{I}$. With simple mathematical derivations, the elements of the matrix \mathbb{P} can be determined as $p_{11} = \frac{1}{2\hbar_{\phi_1}}(1 + \hbar_{\phi_2})$, $p_{12} = p_{21} = -\frac{1}{2}$, and $p_{22} = \frac{1}{2\hbar_{\phi_2}}\left(\frac{1}{\hbar_{\phi_1}}(1 + \hbar_{\phi_2}) + \hbar_{\phi_1}\right)$. Next, taking the derivative of V_H and simplifying it along with using Young's inequality yields:

$$\begin{aligned} \dot{V}_H &= -\chi_\phi^T \chi_\phi + 2\varepsilon \chi_\phi^T \mathbb{P} \delta \\ &\leq -\left(1 - \frac{\varepsilon^2}{2}\right) \chi_1^2 - \left(1 - \frac{\varepsilon^2}{2\hbar_{\phi_2}^2} \left(\frac{1}{\hbar_{\phi_1}}(1 + \hbar_{\phi_2}) + \hbar_{\phi_1}\right)\right) \chi_2^2 + \tilde{f}^2 \end{aligned} \tag{49}$$

Hence, stable dynamics can be achieved by an appropriate choice of $\hbar_{\phi_1} > 0$, $\hbar_{\phi_2} > 0$ and by designing $\varepsilon \in (0, 1]$ to be sufficiently small.

Corollary 2 ([77]). *The state variables in the controller, adaptive laws, and nonlinear DO are replaced with estimated state variables derived using a HGO to finalize the control methodology.*

Theorem 1. *The roll submodel subject to nonlinear disturbance presented in (7) ultimately achieves boundedness uniformly, provided that the nonlinear disturbance observer is designed using (8) and the controller as follows:*

$$\begin{aligned} U_\phi &= \left(\frac{1}{B_\phi^T B_\phi}\right) B_\phi^T (A_1 X_\Phi - F_\phi(t) + B_1(\hat{K}_\phi(t)X_\phi + \hat{K}_{r_\phi}(t)r(t) \\ &\quad - \hat{K}_{v_\phi}(t)\bar{u}_\phi(t))) \end{aligned} \tag{50}$$

where adaptive control gains are chosen according to (31), and $\bar{u}_\phi(t)$ is designed according to (38) with tuning gains according to (40) and state-estimation according to (48).

Proof. Define a Lyapunov function as follows:

$$\begin{aligned} V_R &= V_S + V_\phi + V_H + V_D \\ &= \frac{1}{2} S_\phi^2 + \frac{1}{2\gamma_\phi} \tilde{L}_\phi^2 + \frac{1}{2\eta_\phi} \tilde{K}_\phi^2 + e_\phi^T P e_\phi + c_\phi \left(\tilde{K}_\phi \Gamma_\phi^{-1} \tilde{K}_\phi^T + \frac{1}{\alpha_\phi} \tilde{K}_r^2 + \frac{1}{\beta_\phi} \tilde{K}_v^2 \right) \\ &\quad + \chi_\phi^T \mathbb{P} \chi_\phi + \frac{1}{2} \tilde{d}_\phi^2 \end{aligned} \tag{51}$$

Time derivative is obtained as follows:

$$\begin{aligned} \dot{V}_R &= S_\phi \dot{S}_\phi - \frac{1}{\gamma_\phi} \tilde{L}_\phi \dot{\tilde{L}}_\phi - \frac{1}{\eta_\phi} \tilde{K}_\phi \dot{\tilde{K}}_\phi + \left(e_\phi^T P \dot{e}_\phi + e_\phi^T P \dot{e}_\phi \right) + c_\phi \left(2\tilde{K}_\phi \Gamma_\phi^{-1} \dot{\tilde{K}}_\phi \right. \\ &\quad \left. + \frac{2}{\alpha_\phi} \tilde{K}_r \dot{\tilde{K}}_r + \frac{2}{\beta_\phi} \tilde{K}_v \dot{\tilde{K}}_v \right) - \chi_\phi^T \chi_\phi + 2\varepsilon \chi_\phi^T \mathbb{P} \delta - \mu_\phi \tilde{d}_\phi^2(t) \end{aligned} \tag{52}$$

Introducing the designed adaptive laws and controller followed by simplification yields

$$\dot{V}_R \leq -L_\phi |S_\phi| - K_\phi S_\phi^2 - e_\phi^T Q_\phi e_\phi - \kappa_1 \chi_1^2 - \kappa_2 \chi_2^2 - \mu_\phi \tilde{d}_\phi^2(t) + \zeta \tag{53}$$

where ζ is a maximum bound, such that $\zeta = \max\{\gamma_\phi + \bar{b} + \tilde{f}^2\}$ and

$$\begin{aligned} \kappa_1 &= (1 - \varepsilon^2/2) \\ \kappa_2 &= (1 - \varepsilon^2 / (2\hbar_{\phi_2}^2)) \left((1/\hbar_{\phi_1})(1 + \hbar_{\phi_2}) + \hbar_{\phi_1} \right) \end{aligned} \tag{54}$$

Hence, with the appropriate selection and design of controller gains, the time derivative of the Lyapunov candidate function, \dot{V}_R , is shown to be negative semi-definite. This ensures that the Lyapunov function $V_R(t)$ is non-increasing along the system trajectories, implying that the system state remains bounded. Furthermore, by invoking the properties of Lyapunov stability theory, this result guarantees that the trajectories of the closed-loop system converge to and remain within an invariant neighborhood of the origin.

As $t \rightarrow \infty$, the system state converges to a bounded region around the origin, determined by the level sets of the Lyapunov function. This demonstrates the uniformly ultimately bounded (UUB) stability of the system under the designed control law. Hence, the stability analysis is complete, and the proof is concluded. \square

With the similar control design, the controllers for pitch and yaw can be constructed. The complete algorithm of attitude control is given in Algorithm 1.

Algorithm 1 Attitude Control

Require: Quadrotor parameters and desired attitude: $\phi_{des}(t), \theta_{des}(t), \psi_{des}(t)$

Ensure: Tracking error $\rightarrow 0$: $\phi_{des}(t) \leftarrow \phi(t), \theta_{des}(t) \leftarrow \theta(t), \psi_{des}(t) \leftarrow \psi(t)$

```

1: while Attitude error  $\neq 0$  do
2:   for  $i \in (\phi, \theta, \psi), j \in (1, 3, 5)$  and  $m \in (1, 2, 3)$  do
3:      $\hat{d}_i = z_i + w_i; \hat{z}_i = \mu_i(f_i + c_i U_i + w_i + z_i); w_i = \mu_i x_{j+1}(t)$ 
4:      $X_i = [x_j \ x_{j+1}]^T, F_i = [x_{j+1} \ f_i]^T, B_j = [0 \ c_i]^T, D_i = [0 \ 1]^T$ 
5:      $A_m = [0 \ 1; k_m \ k_{m+1}], B_m = [0 \ k_{m+2}]^T$ 
6:      $\hat{K}_i^T(t) = -\Gamma_i X_i e_i^T \bar{P}_{j+1}; \hat{K}_{r_i}(t) = -\alpha_i k_{m+2} r_i(t) e_i^T \bar{P}_{j+1},$ 
        $\hat{K}_{v_i}(t) = -\beta_i k_{m+2} \bar{u}_i(t) e_i^T \bar{P}_{j+2}$ 
7:      $\hat{Z}_i = \mathbb{P}_i Z_i, \hat{\mathbb{E}}_i = \mathfrak{R}_i \mathbb{E}_i + \mathbb{X}_i$ 
8:      $\hat{X}_\phi = \hat{F}_\phi(t) + B_\phi U_\phi + \mathbb{K}(y_\phi - \hat{x}_1)(t)$ 
9:      $\bar{u}_i = -(C_i^T B_i)^{-1} \left( C_i^T (A_i X_i + D_i \hat{d}_i(t) - \mathbb{P}_i Z_i - \mathfrak{R}_i \mathbb{E}_i - \mathbb{X}_i) \right.$ 
        $\left. + \hat{L}_i \text{sgn}(S_i) + \hat{K}_i S_i \right), \hat{K}_i = \beta_i S_i^2, \hat{L}_i(t) = \alpha_i |S_i|$ 
10:     $v_i(t) = \hat{K}_i(t) X_i + \hat{K}_{r_i}(t) r_i(t) - \hat{K}_{v_i}(t) \bar{u}_i(t)$ 
11:     $U_i(t) = \left( \frac{1}{B_i^T B_i} \right) B_i^T \{ A_m X_i - F_i(t) + B_m v_i \}$ 
12:  if Attitude error  $\rightarrow 0$  then
13:    Stop
14:  else
15:    Redesign control gains and reference model
16:  Repeat

```

3.2. Position Control

Unlike the attitude submodel, the position model of the quadrotor system represents an underactuated system with one input and three outputs. To facilitate the control design, position virtual control inputs are defined as $U(t) = [U_x(t), U_y(t), U_z(t)]^T = -gz + \frac{U_p}{m} Rz$ [2]. Each virtual control input corresponds to the position along the X-axis, Y-axis, and Z-axis, respectively.

Without loss of generality, the state-space representation of the position dynamics along the X-axis is expressed as follows:

$$\begin{aligned} \dot{x}_7(t) &= x_8(t) \\ \dot{x}_8(t) &= U_x(t) + d_x(t) \end{aligned} \tag{55}$$

where $d_x(t)$ is the disturbance acting on the position along the X-axis. The disturbance estimation is given by $\hat{d}_x(t) = z_x(t) + w_x(t)$, where

$$\begin{aligned} \dot{z}_x(t) &= -\mu_x(U_x(t) + u_x(t) + z_x(t)) \\ w_x(t) &= \mu_x x_8(t) \end{aligned} \tag{56}$$

Defining the estimation error as $\tilde{d}_x = d_x(t) - \hat{d}_x(t)$. Its error dynamics can be obtained as $\dot{\tilde{d}}_x = -\mu_x \tilde{d}_x + \frac{1}{2} \tilde{d}_x$, where $\tilde{d}_x \geq \max\{1 + d_x^2\}$. Next, (55) can be written as follows:

$$\dot{X}_x = F_x(t) + B_x U_x + D_x d_x(t) \tag{57}$$

where

$$X_x = [x_7(t) \quad x_8(t)]^T; F_x(t) = [x_8(t) \quad 0]^T; B_x = [0 \quad 1]^T; D_x = [0 \quad 1]^T \tag{58}$$

For this system, the auxiliary control input for position along X-axis is designed as follows:

$$U_x(t) = \left(\frac{1}{B_x^T B_x} \right) B_x^T \{A_4 X_x - F_x(t) + B_4 v_x(t)\} \tag{59}$$

where $A_4 = [0 \ 0; k_{10} \ k_{11}]$ and $B_4 = [0 \ k_{12}]^T$, where k_{10} , k_{11} , and k_{12} are positive constants. Now, for (59), v_x is designed as follows:

$$v_x(t) = \hat{K}_x(t) X_x + \hat{K}_{r_x} r_x(t) - \hat{K}_{v_x}(t) \bar{u}_x(t) \tag{60}$$

Defining a reference model as follows:

$$\dot{X}_{m_x} = A_{m_x} X_{m_x} + B_{m_x} r_x(t) \tag{61}$$

Error between the real and reference model is given by

$$e_x = X_x - X_{m_x} \tag{62}$$

Next, define the Lyapunov function as follows:

$$V_x = e_x^T P_x e_x + \left(\tilde{K}_x(t) \Gamma_x^{-1} \tilde{K}_x^T(t) + \frac{1}{\alpha_x} \tilde{K}_{r_x}^2(t) + \frac{1}{\beta_x} \tilde{K}_{v_x}^2(t) \right) \tag{63}$$

where $P_x A_x + A_x^T P_x = -Q_x$, $P_x = P_x^T$, and $Q_x = Q_x^T$. Furthermore, $\tilde{K}_x = K_x - \hat{K}_x(t)$, $\tilde{K}_{r_x} = K_{r_x} - \hat{K}_{r_x}(t)$, and $\tilde{K}_{v_x} = K_{v_x} - \hat{K}_{v_x}(t)$. Now, taking the derivative of (63) and using (61), the adaptive laws are designed as follows:

$$\dot{\tilde{K}}_x^T(t) = -\Gamma_x X_x e_x^T \bar{P}_8; \dot{\tilde{K}}_{r_x}(t) = -\alpha_x k_{12} r_x(t) e_x^T \bar{P}_8; \dot{\tilde{K}}_{v_x}(t) = -\beta_x k_{12} \bar{u}_x(t) e_x^T \bar{P}_8 \tag{64}$$

where \bar{P}_8 is the second column of P_x that satisfies $P_x A_x + A_x^T P_x = -Q_x$, $P_x = P_x^T$, and $2e_x^T P_x B_x = 2k_{12} e_x^T \bar{P}_8 \in R$. Furthermore, α_x , β_x , k_{12} and $\Gamma_x = \Gamma_x^T \in R^{2 \times 2}$ are positive design constants. Now, using (64), \dot{V}_x can be obtained as follows:

$$\dot{V}_x \leq -e_x^T Q_x e_x + 2e_x^T \bar{P}_8 (k_{12}^2 + 1) + \bar{b}_x \tag{65}$$

where $\bar{b}_x \geq \frac{1}{2} \max\{\bar{u}_x^2(t) + d_x^2(t)\}$ is an upper bound on SMC and disturbance. Hence, uniformly ultimately boundedness can be guaranteed provided that P_x and the control gains are designed appropriately.

In the next step, prior to the design of $\bar{u}_x(t)$, a commanded-filter and its error compensation are designed for obtaining the numerical differentiation of desired trajectory, written as follows:

$$\dot{Z}_x = P_x Z_x; \dot{E}_x = \mathfrak{R}_x E_x + \mathbb{X}_x \tag{66}$$

where in matrix form, it is given as follows:

$$\begin{bmatrix} \dot{z}_7 \\ \dot{z}_8 \end{bmatrix} = \begin{bmatrix} -p_7|z_7 - x_r|^{1/2} & 1 \\ -p_8 & 0 \end{bmatrix} \begin{bmatrix} \text{sign}(z_7 - x_r) \\ z_8 \end{bmatrix}; \tag{67}$$

where x_r is the desired position along the X-axis. $p_1 > 0$ and $p_2 > 0$ are constants. In addition, $z_7 = x^c$ and $z_8 = \dot{x}^c = \dot{x}_r$, and

$$\begin{bmatrix} \dot{\zeta}_7(t) \\ \dot{\zeta}_8(t) \end{bmatrix} = \begin{bmatrix} -r_7 & 1 \\ -1 & -r_8 \end{bmatrix} \begin{bmatrix} \zeta_7 \\ \zeta_8 \end{bmatrix} + \begin{bmatrix} (x^c(t) - x_r) \\ 0 \end{bmatrix} \tag{68}$$

where $r_7 > 0$ and $r_8 > 0$ are the design constants. Next, the sliding manifold is chosen as follows:

$$S_x = C_x^T (X_x - Z_x - E_x) \tag{69}$$

where $C_x = [c_1; 1]$. Next, the sliding mode surface dynamics are obtained as follows:

$$\dot{S}_x = C_x^T (A_x X_x + B_x \bar{u}_x + D_x d_x - P_x Z_x - \mathfrak{R}_x E_x - \mathbb{X}_x) \tag{70}$$

Hence, the control input is chosen as follows:

$$\begin{aligned} \bar{u}_x = & - \left(C_x^T B_x \right)^{-1} \left(C_x^T \left(A_x X_x + D_x \hat{d}_x(t) - P_x Z_x - \mathfrak{R}_x E_x - \mathbb{X}_x \right) \right. \\ & \left. + \hat{L}_x \text{sgn}(S_x) + \hat{K}_x S_x \right) \end{aligned} \tag{71}$$

State estimation of the position submodel using HGO is given by $\dot{\hat{X}}_x = F_x(t) + B_x U_x + \mathbb{K}(y_x - \hat{x}_7)$, where $y_x = x_7$ is the position along the X-axis and

$$\hat{X}_x = [\hat{x}_7 \quad \hat{x}_8]^T; F_x(t) = [x_8 \quad 0]^T; B_x = [0 \quad 1]^T; \mathbb{K}_x = \frac{1}{\varepsilon^2} \begin{bmatrix} \varepsilon \hat{h}_{x_1} & 0 \\ 0 & \hat{h}_{x_2} \end{bmatrix} \tag{72}$$

where $\varepsilon = (0, 1]$, $\hat{h}_{\phi_1} > 0$ and \hat{h}_{ϕ_2} are estimation gains. This finalises the control design of U_x . Using a similar procedure, the controller for the position along the Y-axis and Z-axis, i.e., U_y and U_z , respectively, can be designed.

Using these virtual control inputs, the position control input is formulated as follows:

$$U_p(t) = \frac{m(U_z(t) + g)}{\cos \phi_{\text{des}}(t) \cos \theta_{\text{des}}(t)} \tag{73}$$

where the desired attitude angles are obtained as follows:

$$\begin{aligned} \theta_{\text{des}}(t) &= \tan^{-1} \left(\frac{U_x(t) \cos \psi_{\text{des}}(t) + U_y \sin \psi_{\text{des}}(t)}{U_z(t) + g} \right) \\ \phi_{\text{des}}(t) &= \tan^{-1} \left(\cos \theta_{\text{des}}(t) \frac{(U_x(t) \sin \psi_{\text{des}}(t) - U_y(t) \cos \psi_{\text{des}}(t))}{U_z(t) + g} \right) \end{aligned} \tag{74}$$

where ψ_{des} is a known desired yaw angle. Figure 2 shows the block diagram of simultaneous operation of the position and attitude control inputs.

Remark 3. The virtual position control inputs are used to obtain the desired attitude angles.

Remark 4. There is no singularity in (73) because $\phi_{des}(t)$ and $\theta_{des}(t)$ satisfy $(-\frac{\pi}{2}, \frac{\pi}{2})$.

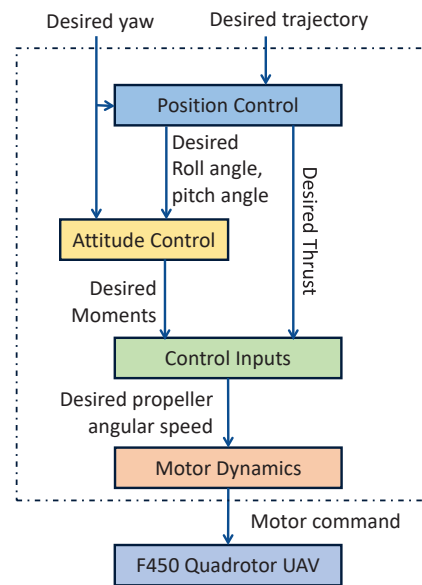


Figure 2. Architecture of cascaded position and attitude control.

Theorem 2. For the underactuated quadrotor model (5) subject to bounded unknown disturbances, the tracking error, disturbance estimation error, and state-estimation error converge and stay in the neighborhood of origin, provided that the attitude controller is designed according to Algorithm 1 and the position controller according to (73).

Proof. The proof follows similar steps to Theorem 1. Hence, it is omitted here. \square

4. Simulation Study

In this section, a simulation study is conducted to evaluate the performance of the proposed controller. A real DJI F450 quadrotor UAV is modeled and simulated in MATLAB using the control strategy developed in this work. The numerical values of the quadrotor’s physical parameters are provided in Table 1. Furthermore, the performance of the proposed controller is compared with the controller presented in [38] to validate its effectiveness and demonstrate its advantages. The closed-loop block diagram of numerical simulations is shown in Figure 3.

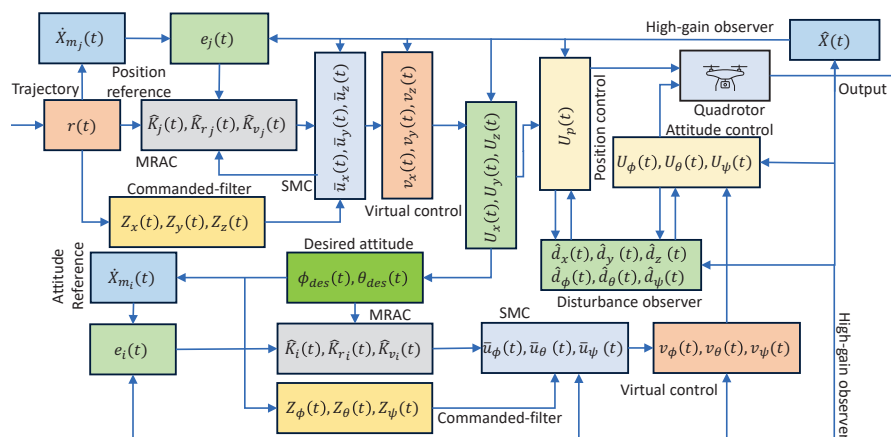


Figure 3. Block diagram of the closed-loop system— $i \in (\phi, \theta, \psi)$, $j \in (x, y, z)$.

4.1. Setup of Desired Trajectories and Nonlinear Disturbances

4.1.1. Desired Trajectories

The desired trajectories can be expressed using $r(t) = [x_{des}(t) \ y_{des}(t) \ z_{des}(t)]^T$. For simulations, two types of trajectories are assumed, i.e., aggressive maneuvers and non-aggressive maneuvers. For aggressive maneuvers, Lissajous trajectory is assumed with $x_{des}(t) = 5 \sin(at)$, $y_{des}(t) = 5 \sin(bt)$, and $z_{des}(t) = 5 \sin(ct) + 5$, where $a = 6\pi/t_f$, $b = 4\pi/t_f$, and $c = 2\pi/t_f$ with $t_f = 180$. For non-aggressive maneuvers, $x_{des}(t) = 0.1 + 0.05t \sin(\frac{t}{\pi})$, $y_{des}(t) = 0.1 + 0.05t \cos(\frac{t}{\pi})$, and $z_{des}(t) = 0.2 + 0.05t$.

4.1.2. Nonlinear Disturbances

The quadrotor UAV is an underactuated system with four inputs and six outputs. In this research work, it is assumed that each quadrotor output is opposed by a different type of disturbance, i.e., during flight mode, the quadrotor experiences six different disturbances. It is assumed that the disturbances in the position model are exogenous disturbance, constant disturbance, and nonlinear disturbance, with variable frequencies and magnitudes, mathematically expressed as $d_x(t) = \Pi_x \Xi_x$; $\dot{\Xi}_x = \frac{1}{\kappa_\phi} \Phi_x \Xi_x$, $d_y(t) = \kappa_y \forall t > t_y$, and $d_z(t) = v + k_z t_z$; $k_z = (f_1 - f_0)/T$, respectively, where $\Pi_x = [0 \ 1]$, $\Phi_x = [0 \ \omega_x; -\omega_x \ 0]$ where $\omega_x = 0.1$. Furthermore, $[\kappa_x, \kappa_y, \kappa_z]^T = [1, 1, 0.1]^T$ and $v = 1$. Moreover, the initial and final frequencies of nonlinear disturbance are $f_0 = 10^{-1}$ and $f_1 = 10^{-3}$, respectively.

To model the disturbances appearing in the attitude model, Simulink built-in blocks were employed. It was assumed that the attitude model faces disturbances in the form of Gaussian-distributed random disturbance in the roll model with zero mean, and variance = 1. Furthermore, uniformly distributed random disturbance in the pitch model exists with a peak-to-peak magnitude of 0.5 and a seed value of 0.5. Moreover, band-limited white noise in yaw model with noise power of 0.05. Since these disturbance are discrete, the sampling time is 1 s.

4.2. Trajectory Tracking Simulations

Table 2 presents the control parameters employed in the design of the controller developed in this research. The feedback gains for the attitude submodel are set as $k_i = k_{i+1} = k_{i+2} = 50$, where $i \in \{1, 4, 7\}$, corresponding to roll, pitch, and yaw dynamics, respectively. For the position control along the x , y , and z axes, the feedback gains are chosen as $k_j = k_{j+1} = k_{j+2} = 1$, where $j \in \{10, 14, 17\}$. Additionally, the reference model is uniformly designed across all submodels with a damping ratio $\zeta = \frac{1}{4}$ and a natural frequency $\omega = 4$. These parameter selections ensure robust control performance and consistent trajectory tracking under varying dynamic conditions.

Table 2. Design control parameters for aggressive maneuvers.

Model	MRAC			Commanded-Filter		SMC			HGO		
	Γ_{11}	Γ_{22}	α	β	$[p_1, p_2]$	$[r_1, r_2]$	γ	η	c	\hat{h}_1	\hat{h}_2
Attitude	10^{-3}	0.1	0.1	0.01	[1, 1]	[5, 1]	1	30	120	1	2
	10^{-3}	0.1	0.1	0.01	[1, 1]	[5, 1]	1	20	100	1	2
	10^{-3}	0.1	0.1	0.01	[1, 1]	[5, 1]	1	20	100	1	2
Position	10^{-4}	0.01	0.01	0.02	[1, 1]	[5, 1]	20	1	5	1	2
	10^{-3}	0.01	0.01	0.08	[1, 1]	[5, 1]	15	30	0	1	2
	10^{-4}	0.01	0.001	0.02	[1, 1]	[5, 1]	5	50	1	1	2

4.2.1. Aggressive Trajectory Tracking

For the simulation, it was assumed that the DJI F450 quadrotor was initially placed on the ground and started from the origin for both trajectory scenarios. During the simulations of aggressive maneuvers, specifically the Lissajous trajectory, the quadrotor accurately followed the desired path, as illustrated in the 3D trajectory tracking plot shown in Figure 4.

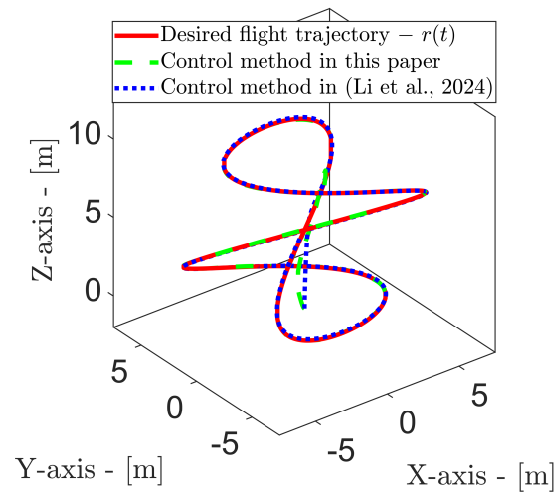


Figure 4. Trajectory tracking—aggressive maneuvers [38].

The phase portraits of the quadrotor's velocity with respect to its position are presented in Figure 5. In the phase portraits for $x(t)$ and $y(t)$, the elliptical trajectories indicate periodic motion, which reflects the oscillatory movement of the quadrotor in the x - y plane. The vectors in these plots highlight the cyclic nature of the quadrotor's motion, where the velocity increases as it moves away from the origin and decreases as it returns. Moreover, the abrupt transitions observed in the phase portrait of $z(t)$ reflect the quadrotor's rapid ascents and descents, effectively following the aggressive nature of the trajectory.

These results validate the performance of the proposed controller, showcasing its capability to achieve coordinated motion and precise positioning while navigating through aggressive maneuvers. The trajectory tracking accuracy and stability evident in the plots further emphasize the effectiveness of the control strategy developed in this research.

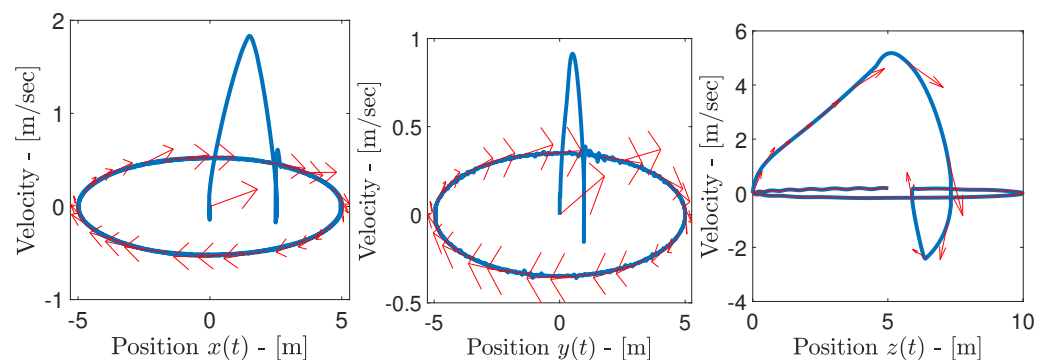


Figure 5. Phase portraits—aggressive maneuvers.

4.2.2. Helical Trajectory Tracking

In the second case of trajectory tracking, the quadrotor demonstrates effective tracking of the desired helical trajectory, as illustrated in Figure 6. In this scenario, the quadrotor successfully follows the dynamically varying positions along the $x(t)$ and $y(t)$ axes, while simultaneously ascending and accurately tracking the desired $z(t)$. The trajectory progres-

sively increases along all three axes, and despite this, the quadrotor effectively adheres to the desired path, showcasing the robustness of the control system.

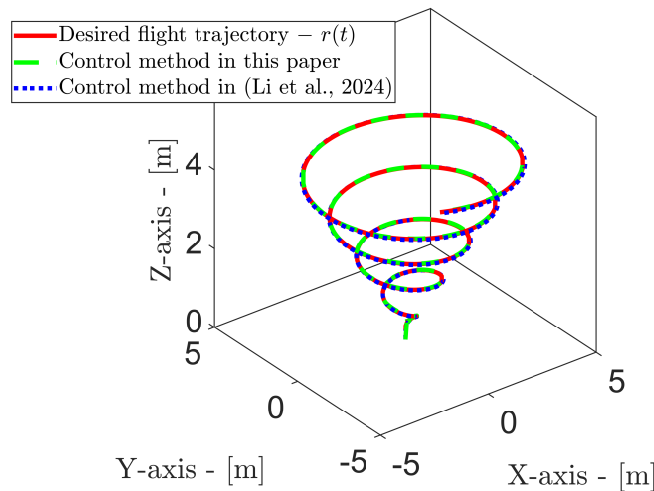


Figure 6. Trajectory tracking—helical [38].

The phase portraits for the helical trajectory tracking are presented in Figure 7. The symmetrical patterns observed in the phase portraits of $x(t)$ and $y(t)$ indicate consistent and stable oscillations, gradually expanding outward as the trajectory evolves. In contrast, the phase portrait for $z(t)$ demonstrates a steady-state response, with unidirectional vectors signifying smooth vertical ascent. The initial oscillations in the phase portraits reflect the transient response phase before the quadrotor effectively stabilizes and tracks the desired helical trajectory.

These results confirm that the quadrotor responds well to the proposed controller and achieves the desired trajectory tracking objectives, showcasing its capability to handle varying positional and altitude demands.

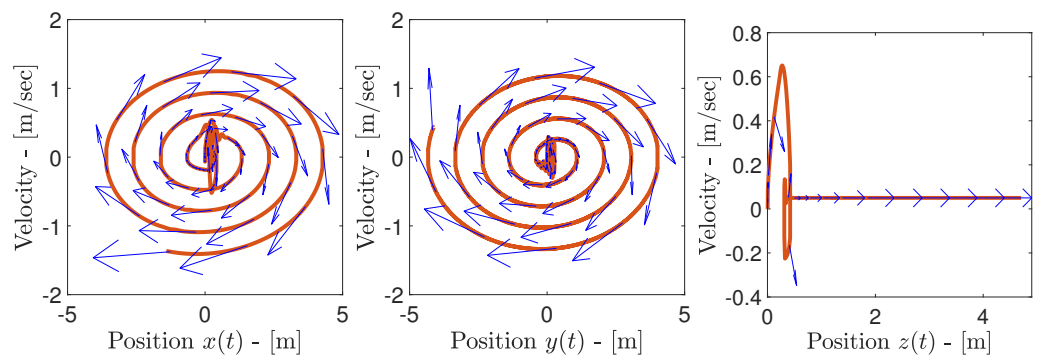


Figure 7. Phase portraits—helical trajectory.

To avoid a repetition of similar simulation results, only the tracking control results for aggressive maneuvers, specifically the Lissajous trajectory, are presented. Figures 8 and 9 illustrate the point-to-point tracking of the quadrotor’s position and attitude, respectively. The plots compare the real and estimated quadrotor outputs against the outputs obtained using the controller designed in [38]. For the attitude tracking, the effects of internal disturbances are noticeable. However, due to the robust and adaptive nature of the proposed controller, the position output effectively attenuates these disturbances and achieves accurate tracking of the desired trajectory.

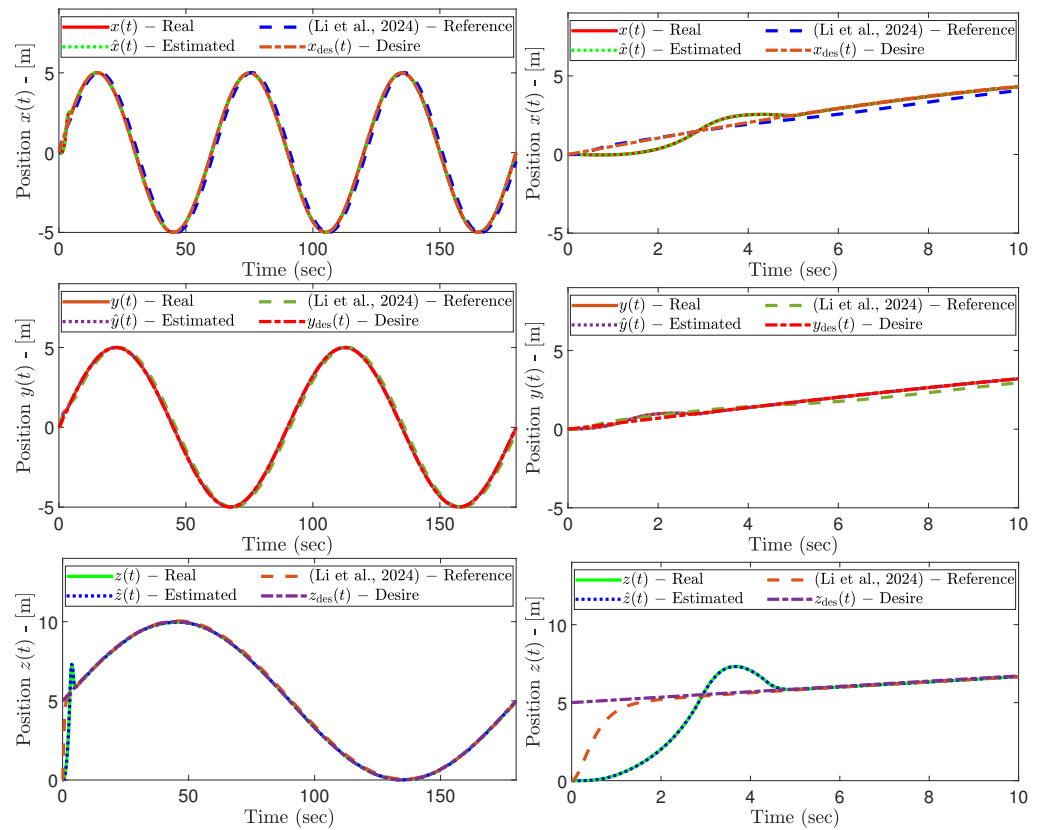


Figure 8. Quadrotor position tracking—aggressive maneuvers [38].

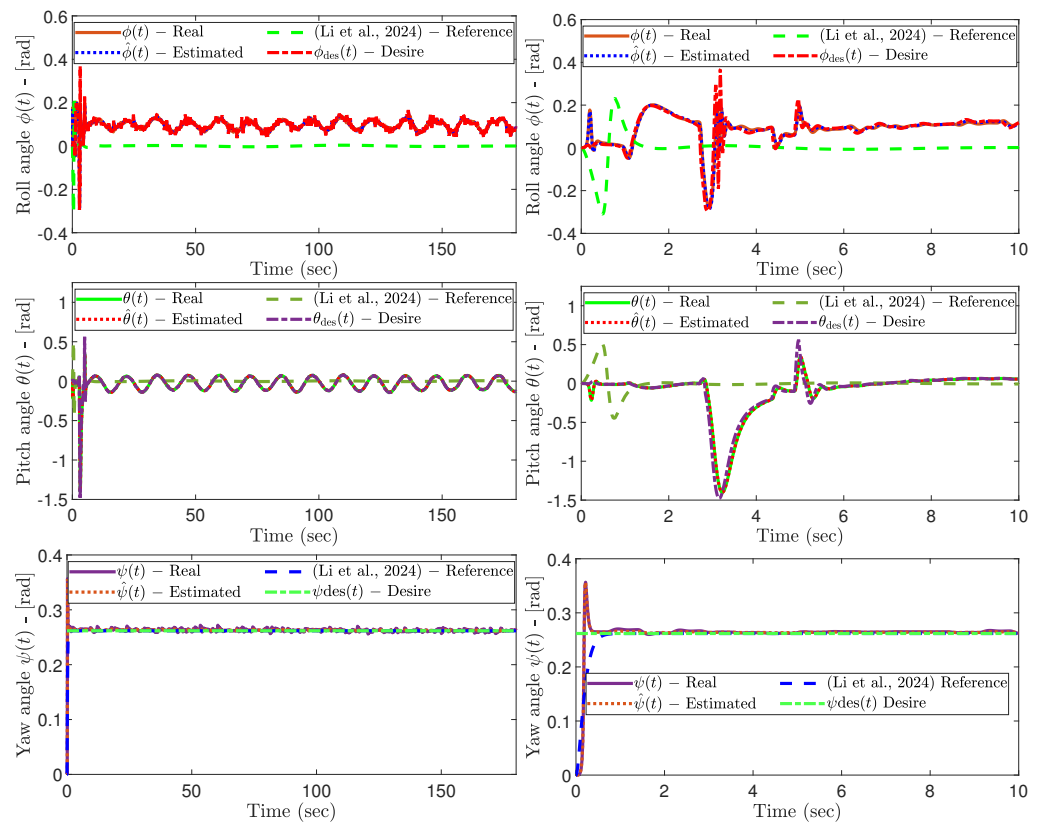


Figure 9. Quadrotor attitude tracking—aggressive maneuvers [38].

When tracking the aggressive maneuvers starting from the origin, the proposed controller demonstrates a slight overshoot before settling into effective tracking performance. This transient behavior is influenced by the design of the reference model, which is depen-

dent on the damping ratio and natural frequency. Despite this, the controller achieves a significant reduction in the root mean square error (RMSE) of tracking errors, as shown in Figure 10.

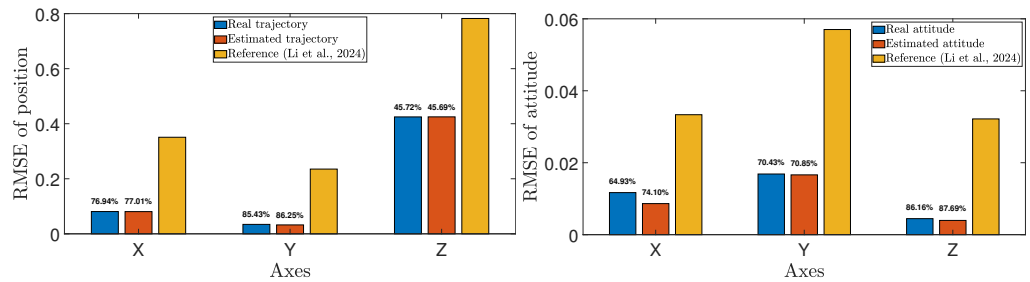


Figure 10. RMSE during aggressive maneuvers [38].

4.3. 3D Visualisation of RMSE

Figure 11 presents the slice-plots of the tracking errors, focusing on regions where the RMSE exceeds the threshold of 1. A symmetric behavior is observed in the tracking errors of the position controller, which can be attributed to the aggressive maneuvers defined by the Lissajous trajectory. Initially, as the quadrotor ascends from the origin to the starting point of the trajectory, significant tracking errors are evident. However, these errors diminish over time as the system stabilizes, demonstrating the quadrotor’s performance and the convergence of errors to a steady state.

Similarly, the RMSE of the quadrotor’s attitude is effectively regulated. While transient deviations are observed during initial phases, these systematically reduce over time, underscoring the robustness of the proposed controller in managing and attenuating disturbances.

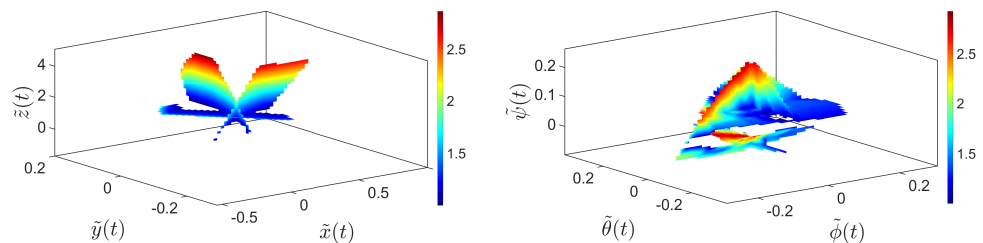


Figure 11. Error visualization for quadrotor attitude and position during trajectory tracking.

In Figure 12, a 3D visualization of the quadrotor outputs is presented for regions where the RMSE exceeds the threshold of 2. The gradual flattening of the RMSE for the quadrotor’s position demonstrates that the position errors converge as the controller successfully achieves trajectory tracking. In contrast, while the RMSE of the quadrotor’s attitude appears more scattered, it also converges and remains within a small vicinity of the threshold over time. The isosurfaces highlight that the errors consistently stay below the specified threshold throughout the tracking task, thereby validating the proposed controller’s capability to maintain bounded and reliable tracking performance.

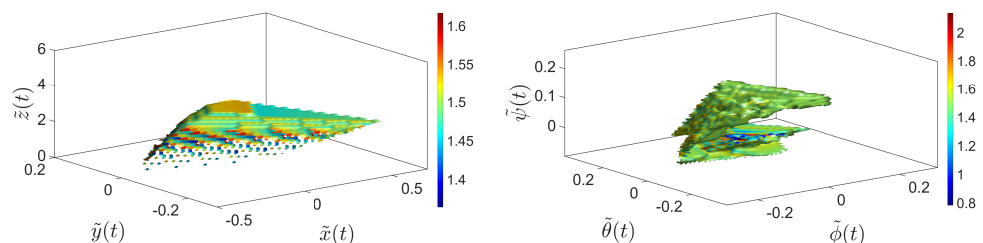


Figure 12. Error distribution in quadrotor attitude and position tracking visualized through isosurfaces.

4.4. Disturbance Estimation

In this research work, the flight of the quadrotor UAV is assumed to be influenced by both external and internal disturbances affecting its position and attitude, respectively. As a 6-degree-of-freedom system, each submodel of the quadrotor is subject to distinct disturbances. For the position model, exogenous disturbances, constant disturbances, and nonlinear disturbances with unknown frequency and magnitude are considered. In contrast, the attitude model experiences Gaussian-distributed random disturbances, uniformly distributed random disturbances, and band-limited white noise.

To estimate these disturbances, unlike traditional DOs that are typically tailored for a single type of disturbance, this research introduces a unified DO algorithm capable of estimating all types of disturbances considered in this study. Figure 13 illustrates the disturbance estimation for disturbances appearing in the position model. The initial overshoot observed in the DO for the position model arises from the quadrotor starting at the origin and needing to ascend to the starting point of the aggressive maneuvers trajectory. This ascent induces a transient overshoot in the controller, which is reflected in the DO's response as shown in the zoomed plots.

Figure 14 demonstrates the accurate disturbance estimation for the quadrotor's attitude, where disturbances are modeled using discrete Simulink blocks with predefined sampling times. The simulations reveal that the sampling time can be reduced to even smaller values without compromising the effectiveness of the DO in estimating disturbances. The zoomed-in plot reveals a slight delay in disturbance estimation, which can be minimized by increasing the control gain.

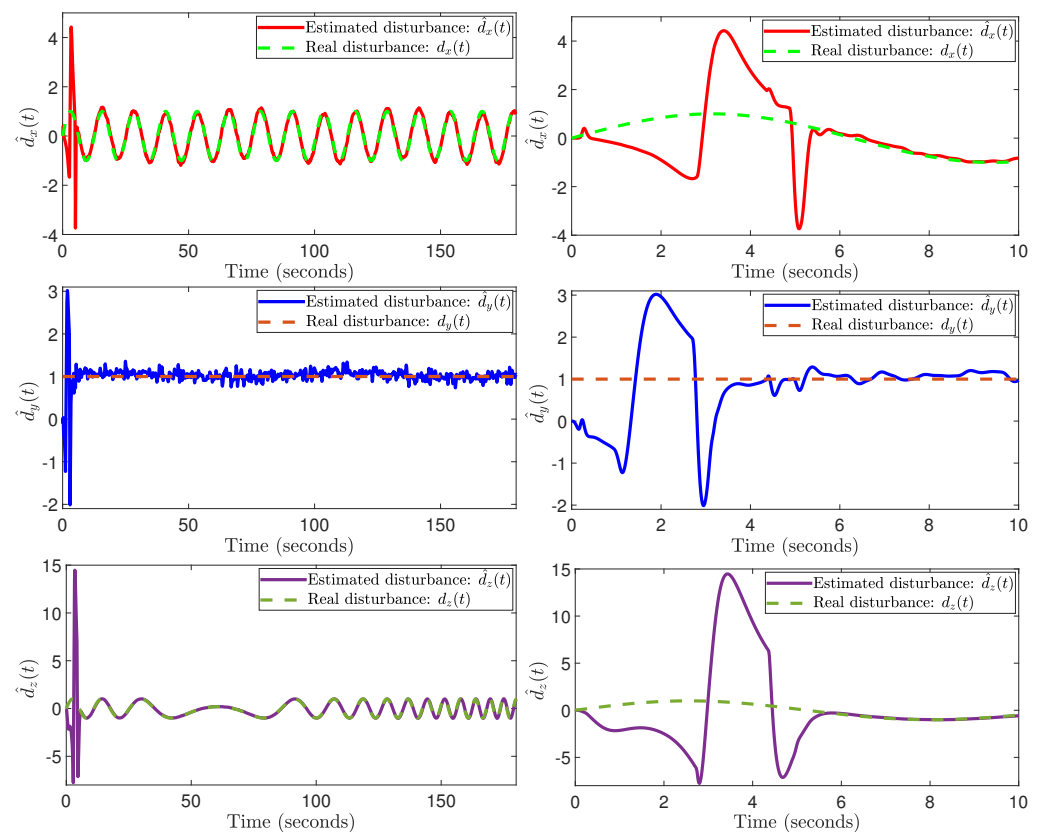


Figure 13. Disturbance estimation in the position model during aggressive maneuvers.

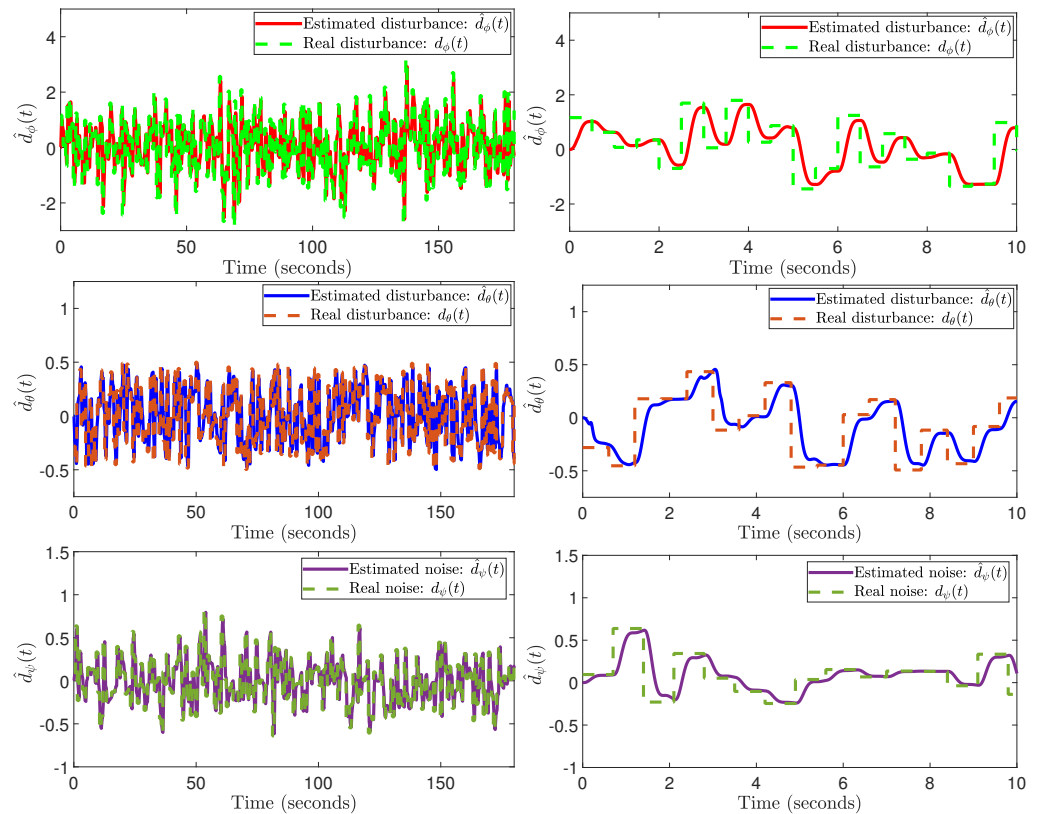


Figure 14. Disturbance estimation in the attitude model during aggressive maneuvers.

4.5. Control Inputs, Forces, and Torques of Rotors

The control inputs for quadrotor position and attitude are illustrated in Figure 15. It is observed that the position control inputs exhibit an initial overshoot, which occurs as the quadrotor ascends from the origin to reach the starting point of the aggressive maneuvers trajectory. Once the quadrotor aligns with the desired trajectory, the control inputs stabilize and achieve a steady state. However, due to the disturbances acting on the position submodel, the control input exhibits fluctuations as it dynamically compensates to ensure that the quadrotor effectively tracks the desired aggressive maneuver trajectory.

In addition to achieving precise position tracking, the position controller also determines the desired attitude, which is subsequently tracked using the attitude control inputs. This hierarchical structure ensures that the position control functions as an outer-loop controller, providing reference signals to the attitude control, which operates as the inner-loop controller. The forces and torques generated by each of the four rotors to implement the control actions are shown in Figure 16.

By utilizing the measured torques and angular velocities of each rotor during simulations of aggressive maneuvers, the total power consumed by the quadrotor is presented in Figure 17. Initially, as the quadrotor ascends rapidly from the origin to reach the desired trajectory, it requires higher power consumption. Once it stabilizes along the trajectory, power consumption becomes more uniform. The effects of disturbance attenuation through position control can also be observed in the power consumption plots, where power consumption dynamically adjusts to ensure successful trajectory tracking while executing aggressive maneuvers.

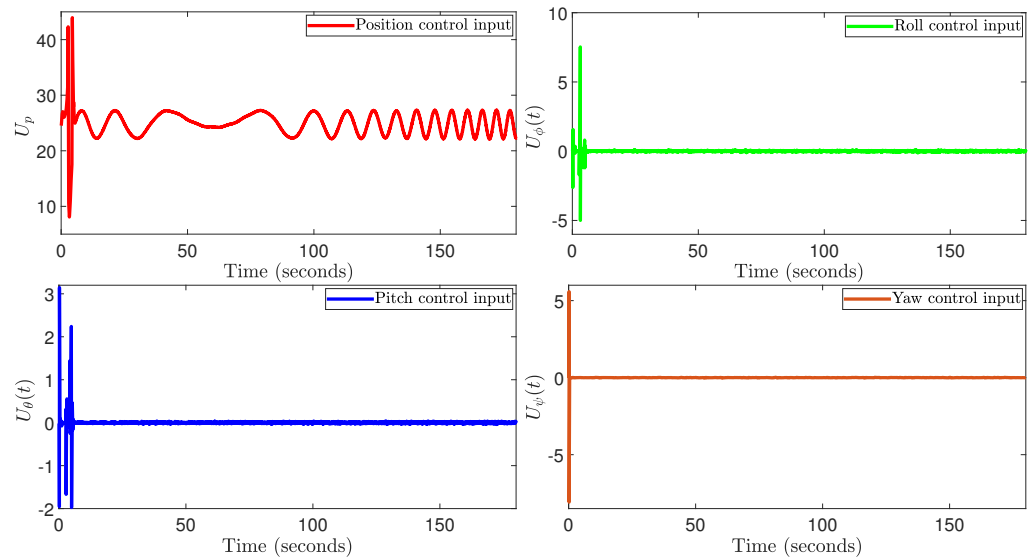


Figure 15. Quadrotor control inputs during aggressive maneuvers.

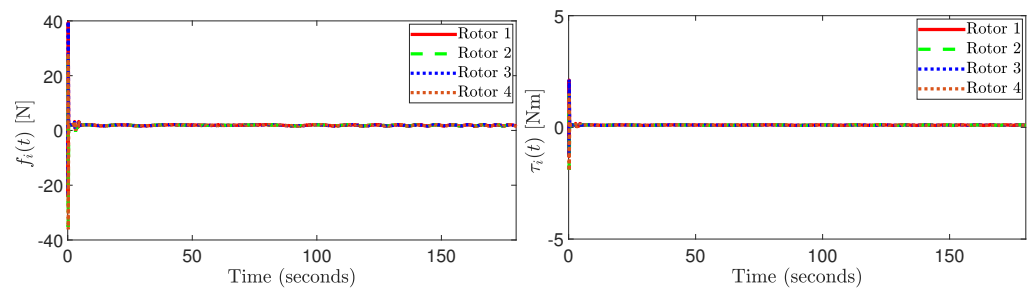


Figure 16. Force and torque of each rotor during aggressive maneuvers.

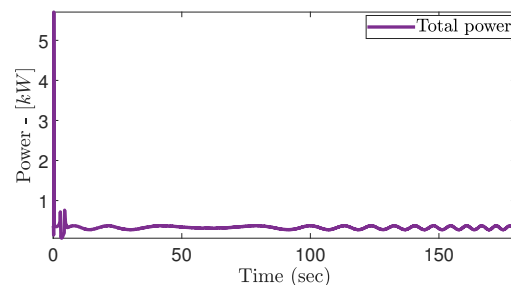


Figure 17. Total power consumed by DJI-F450.

4.6. Discussion on Comparison, Real Experiments, and Limitations

The controller presented in this research addresses critical challenges associated with quadrotor UAV trajectory tracking, including external and internal disturbances, sensor inaccuracies, and the need for robust and adaptive control techniques. To address computational delays in the numerical differentiation of state variables, a commanded-filter with error compensation is utilized. Furthermore, parametric and modeling uncertainties are managed through the introduction of a reference model in the control design. This developed controller is compared with the method proposed in [38] to assess its effectiveness.

Both the proposed controller and the comparison method demonstrate excellent trajectory tracking performance for aggressive and non-aggressive maneuvers. However, the controller in this work exhibits superior performance, achieving reduced RMSE for quadrotor position and attitude, as shown in the bar chart in Figure 10. Furthermore, the comparison method is limited to estimating sinusoidal disturbances, whereas the proposed controller estimates and rejects six distinct types of disturbances encountered

during quadrotor flight, all using a single DO algorithm. Additionally, while the DO in the comparison method requires accurate measurements of state variables and their rates, posing challenges in the presence of sensor faults, the proposed DO utilizes estimated states, thus bypassing issues arising from sensor malfunctions.

The adaptive laws in the proposed controller simplify implementation by autonomously tuning the control gains, eliminating the need for empirical tuning. Conversely, the comparison method relies on manual gain tuning, which must be repeated for every change in trajectory. The reference model employed in this work further enhances robustness by accommodating parametric uncertainties and unmodeled dynamics, ensuring consistent trajectory tracking. In contrast, the comparison method relies on Lyapunov criteria to cancel nonlinear coupled terms, necessitating higher control effort and the repeated differentiation of virtual control inputs and states, which can lead to an *'explosion of complexity'* and potential instability.

Despite its superior performance, the proposed controller shows certain areas for improvement. One challenge is the initial overshoot observed during aggressive maneuvers, influenced by the selection of the reference model's damping ratio and natural frequency. While this overshoot can be reduced through appropriate tuning of these parameters, determining optimal values remains a complex task. Additionally, as the tracking error between the reference model and the real system approaches zero, the adaptive laws within the MRAC framework may yield less precise control gains, which could affect trajectory tracking accuracy under such conditions.

The proposed control technique also relies on a HGO state-estimator, which is limited to integral-chain systems. Designing the HGO gain parameter, $\varepsilon \in (0, 1]$, is another challenge. Noted in simulations, extremely small values of ε can result in high control activity, violating motor dynamics in real-world experiments, and may cause a peaking phenomenon, as highlighted in [68]. A potential future work direction includes improving the accuracy of adaptive laws under near-zero tracking errors, implementing the controller in real-world scenarios, refining the design of the time constant ε , optimizing DO gain, establishing systematic reference model design criteria, and addressing input delays, all of which could further enhance the proposed control framework.

5. Conclusions

This paper presents a robust and adaptive control framework for achieving both aggressive and non-aggressive trajectory tracking of quadrotors in the presence of unknown nonlinear external and internal disturbances. By employing a nonlinear disturbance observer, six distinct types of disturbances were attenuated across various flight modes. The proposed framework integrates a model-reference adaptive control scheme to ensure the accurate replication of a predefined reference model, while a sliding mode control strategy was used to design the tracking error dynamics, enabling precise trajectory tracking under the matching conditions of the adaptive control framework. The controller design incorporates a commanded-filter structure with error compensation to address numerical differentiation challenges and employs a high-gain observer to estimate the quadrotor's states and rates. The stability and convergence of the control laws were rigorously analyzed using Lyapunov methods, ensuring ultimately uniformly bounded stability. The effectiveness of the proposed methodology was validated through simulations on a DJI-F450 quadrotor platform, demonstrating its robustness and applicability to real-world unmanned aerial vehicle systems for reliable trajectory tracking in the presence of complex and uncertain disturbances.

Author Contributions: Formal analysis, N.A. (Nigar Ahmed); Funding acquisition, N.A. (Nashmi Alrasheedi); Investigation, N.A. (Nigar Ahmed); Methodology, N.A. (Nigar Ahmed); Resources, N.A. (Nashmi Alrasheedi); Software, N.A. (Nigar Ahmed); Validation, N.A. (Nashmi Alrasheedi); Writing—original draft, N.A. (Nigar Ahmed); Writing—review & editing, N.A. (Nashmi Alrasheedi). All authors have read and agreed to the published version of the manuscript.

Funding: This work was supported and funded by the Deanship of Scientific Research at Imam Mohammad Ibn Saud Islamic University (IMSIU) (grant number IMSIU-DDRSP2503).

Data Availability Statement: The original contributions presented in this study are included in the article. Further inquiries can be directed to the corresponding author.

Conflicts of Interest: The authors declare no conflicts of interest.

References

- Huang, Y.; Sun, B.; Meng, Z.; Sun, J. Adaptive Formation Tracking Control of Multiple Vertical Takeoff and Landing UAVs with Bearing-Only Measurements. *IEEE Trans. Cybern.* **2024**, *54*, 3491–3501. [[CrossRef](#)] [[PubMed](#)]
- Zuo, Z. Trajectory tracking control design with command-filtered compensation for a quadrotor. *IET Control Theory Appl.* **2010**, *4*, 2343–2355. [[CrossRef](#)]
- Li, J.; Ye, D.H.; Kolsch, M.; Wachs, J.P.; Bouman, C.A. Fast and Robust UAV to UAV Detection and Tracking from Video. *IEEE Trans. Emerg. Top. Comput.* **2022**, *10*, 1519–1531. [[CrossRef](#)]
- Mobayen, S.; El-Sousy, F.F.; Alattas, K.A.; Mofid, O.; Fekih, A.; Rojsiraphisal, T. Adaptive fast-reaching nonsingular terminal sliding mode tracking control for quadrotor UAVs subject to model uncertainties and external disturbances. *Ain Shams Eng. J.* **2023**, *14*, 102059. [[CrossRef](#)]
- Wang, Y.; Lu, Q.; Ren, B. Wind turbine crack inspection using a quadrotor with image motion blur avoided. *IEEE Robot. Autom. Lett.* **2023**, *8*, 1069–1076. [[CrossRef](#)]
- Wang, J.; Alattas, K.A.; Bouteraa, Y.; Mofid, O.; Mobayen, S. Adaptive finite-time backstepping control tracker for quadrotor UAV with model uncertainty and external disturbance. *Aerosp. Sci. Technol.* **2023**, *133*, 108088. [[CrossRef](#)]
- Yu, D.; Ma, S.; Liu, Y.J.; Wang, Z.; Chen, C.P. Finite-time adaptive fuzzy backstepping control for quadrotor UAV with stochastic disturbance. *IEEE Trans. Autom. Sci. Eng.* **2023**, *21*, 1335–1345. [[CrossRef](#)]
- Lopez-Sanchez, I.; Moreno-Valenzuela, J. PID control of quadrotor UAVs: A survey. *Annu. Rev. Control* **2023**, *56*, 100900. [[CrossRef](#)]
- Ata, B.; Gencal, M.C. Comparison of optimization approaches on linear quadratic regulator design for trajectory tracking of a quadrotor. *Evol. Intell.* **2024**, *17*, 3225–3240. [[CrossRef](#)]
- BaniAsad, A.; Pordal, R.; Sharifi, A.; Nobahari, H. Attitude control of a 3-DoF quadrotor platform using a linear quadratic integral differential game approach. *ISA Trans.* **2024**, *148*, 515–527. [[CrossRef](#)]
- Madeiras, J.; Cardeira, C.; Oliveira, P. Trajectory tracking of a quadrotor via full-state feedback control. *Aerosp. Sci. Technol.* **2024**, *147*, 109013. [[CrossRef](#)]
- Surma, C.C.; Barczyk, M. Linear model predictive control for vision-based UAV pursuit. *J. Unmanned Veh. Syst.* **2020**, *8*, 334–363. [[CrossRef](#)]
- Kanai, M.; Yamakita, M. Lifted Bilinear Model-based Linear Model Predictive Control with Scalability. *IFAC-PapersOnLine* **2023**, *56*, 9405–9410. [[CrossRef](#)]
- Petrлік, M.; Báča, T.; Heřt, D.; Vrba, M.; Krajník, T.; Saska, M. A Robust UAV System for Operations in a Constrained Environment. *IEEE Robot. Autom. Lett.* **2020**, *5*, 2169–2176. [[CrossRef](#)]
- Idrissi, M.; Salami, M.; Annaz, F. A review of quadrotor unmanned aerial vehicles: Applications, architectural design and control algorithms. *J. Intell. Robot. Syst.* **2022**, *104*, 22. [[CrossRef](#)]
- Labbadi, M.; Cherkaoui, M. Adaptive fractional-order nonsingular fast terminal sliding mode based robust tracking control of quadrotor UAV with Gaussian random disturbances and uncertainties. *IEEE Trans. Aerosp. Electron. Syst.* **2021**, *57*, 2265–2277. [[CrossRef](#)]
- Nguyen, N.P.; Oh, H.; Moon, J. Continuous nonsingular terminal sliding-mode control with integral-type sliding surface for disturbed systems: Application to attitude control for quadrotor UAVs under external disturbances. *IEEE Trans. Aerosp. Electron. Syst.* **2022**, *58*, 5635–5660. [[CrossRef](#)]
- Raza, A.; Malik, F.M.; Khan, R.; Mazhar, N.; Ullah, H.; Ahmed, N. Sliding mode control-based autonomous control of a tri-rotor unmanned aerial vehicle. *Guid. Navig. Control* **2021**, *1*, 2150013. [[CrossRef](#)]
- Chen, M.; Xiong, S.; Wu, Q. Tracking flight control of quadrotor based on disturbance observer. *IEEE Trans. Syst. Man Cybern. Syst.* **2019**, *51*, 1414–1423. [[CrossRef](#)]

20. Lee, D.; Jin Kim, H.; Sastry, S. Feedback linearization vs. adaptive sliding mode control for a quadrotor helicopter. *Int. J. Control Autom. Syst.* **2009**, *7*, 419–428. [[CrossRef](#)]
21. Shao, X.; Sun, G.; Yao, W.; Liu, J.; Wu, L. Adaptive Sliding Mode Control for Quadrotor UAVs with Input Saturation. *IEEE/ASME Trans. Mechatron.* **2022**, *27*, 1498–1509. [[CrossRef](#)]
22. Smith, S.; Pan, Y.J. Adaptive Observer-Based Super-Twisting Sliding Mode Control for Low Altitude Quadcopter Grasping. *IEEE/ASME Trans. Mechatron.* **2024**, *30*, 587–598. [[CrossRef](#)]
23. Tripathi, V.K.; Kamath, A.K.; Behera, L.; Verma, N.K.; Nahavandi, S. Finite-time super twisting sliding mode controller based on higher-order sliding mode observer for real-time trajectory tracking of a quadrotor. *IET Control Theory Appl.* **2020**, *14*, 2359–2371. [[CrossRef](#)]
24. Naser, H.N.; Hashim, H.A.; Ahmadi, M. Aerial assistive payload transportation using quadrotor UAVs with nonsingular fast terminal SMC for human physical interaction. *Results Eng.* **2025**, *25*, 103701. [[CrossRef](#)]
25. Chandra, A.; Lal, P.P. Higher order sliding mode controller for a quadrotor UAV with a suspended load. *IFAC-PapersOnLine* **2022**, *55*, 610–615. [[CrossRef](#)]
26. Zhang, Y.; Fu, Y.; Han, Z.; Wang, J. Super-Twisting Algorithm Backstepping Adaptive Terminal Sliding-Mode Tracking Control of Quadrotor Drones Subjected to Faults and Disturbances. *Drones* **2025**, *9*, 82. [[CrossRef](#)]
27. Zhao, Z.; Cao, D.; Yang, J.; Wang, H. High-order sliding mode observer-based trajectory tracking control for a quadrotor UAV with uncertain dynamics. *Nonlinear Dyn.* **2020**, *102*, 2583–2596. [[CrossRef](#)]
28. Danesh, M.; Jalalaei, A.; Derakhshan, R.E. Auto-landing algorithm for quadrotor UAV using super-twisting second-order sliding mode control in the presence of external disturbances. *Int. J. Dyn. Control* **2023**, *11*, 2940–2957. [[CrossRef](#)]
29. Shevidi, A.; Hashim, H.A. Quaternion-based adaptive backstepping fast terminal sliding mode control for quadrotor UAVs with finite time convergence. *Results Eng.* **2024**, *23*, 102497. [[CrossRef](#)]
30. Xie, W.; Cabecinhas, D.; Cunha, R.; Silvestre, C. Adaptive backstepping control of a quadcopter with uncertain vehicle mass, moment of inertia, and disturbances. *IEEE Trans. Ind. Electron.* **2021**, *69*, 549–559. [[CrossRef](#)]
31. Bhatia, A.K.; Jiang, J.; Zhen, Z.; Ahmed, N.; Rohra, A. Projection Modification Based Robust Adaptive Backstepping Control for Multipurpose Quadcopter UAV. *IEEE Access* **2019**, *7*, 154121–154130. [[CrossRef](#)]
32. Koksai, N.; An, H.; Fidan, B. Backstepping-based adaptive control of a quadrotor UAV with guaranteed tracking performance. *ISA Trans.* **2020**, *105*, 98–110. [[CrossRef](#)] [[PubMed](#)]
33. Belmouhoub, A.; Medjmadj, S.; Bouzid, Y.; Derrouaoui, S.; Guiatni, M. Enhanced backstepping control for an unconventional quadrotor under external disturbances. *Aeronaut. J.* **2023**, *127*, 627–650. [[CrossRef](#)]
34. Chen, M.; Yan, K.; Wu, Q. Multiapproximator-Based Fault-Tolerant Tracking Control for Unmanned Autonomous Helicopter With Input Saturation. *IEEE Trans. Syst. Man Cybern. Syst.* **2022**, *52*, 5710–5722. [[CrossRef](#)]
35. Niu, Y.; Ban, H.; Zhang, H.; Gong, W.; Yu, F. Nonsingular Terminal Sliding Mode Based Finite-Time Dynamic Surface Control for a Quadrotor UAV. *Algorithms* **2021**, *14*, 315. [[CrossRef](#)]
36. Zhu, G.; Wang, S.; Sun, L.; Ge, W.; Zhang, X. Output feedback adaptive dynamic surface sliding-mode control for quadrotor UAVs with tracking error constraints. *Complexity* **2020**, *2020*, 8537198. [[CrossRef](#)]
37. Ding, J.; Zhang, W. Finite-time adaptive control for nonlinear systems with uncertain parameters based on the command filters. *Int. J. Adapt. Control Signal Process.* **2021**, *35*, 1754–1767. [[CrossRef](#)]
38. Li, S.; Duan, N.; Min, H. Trajectory tracking control for quadrotor unmanned aerial vehicle with input delay and disturbances. *Asian J. Control* **2024**, *26*, 150–161. [[CrossRef](#)]
39. Ahmed, N.; Chen, M. Robust model reference adaptive backstepping sliding-mode control for quadrotor attitude with disturbance observer. *Aircr. Eng. Aerosp. Technol.* **2021**, *93*, 1156–1170. [[CrossRef](#)]
40. Yuksek, B.; Inalhan, G. Reinforcement learning based closed-loop reference model adaptive flight control system design. *Int. J. Adapt. Control Signal Process.* **2021**, *35*, 420–440. [[CrossRef](#)]
41. Ma, C.; Lam, J.; Lewis, F.L. Trajectory Regulating Model Reference Adaptive Controller for Robotic Systems. *IEEE Trans. Control Syst. Technol.* **2019**, *27*, 2749–2756. [[CrossRef](#)]
42. Glushchenko, A.; Lastochkin, K. Quadrotor Trajectory Tracking Using Model Reference Adaptive Control, Neural Network-Based Parameter Uncertainty Compensator, and Different Plant Parameterizations. *Computation* **2023**, *11*, 163. [[CrossRef](#)]
43. Chen, W.H.; Ballance, D.J.; Gawthrop, P.J.; O'Reilly, J. A nonlinear disturbance observer for robotic manipulators. *IEEE Trans. Ind. Electron.* **2000**, *47*, 932–938. [[CrossRef](#)]
44. Wang, F.; Gao, H.; Wang, K.; Zhou, C.; Zong, Q.; Hua, C. Disturbance observer-based finite-time control design for a quadrotor UAV with external disturbance. *IEEE Trans. Aerosp. Electron. Syst.* **2020**, *57*, 834–847. [[CrossRef](#)]
45. Wang, H.; Chen, M. Trajectory tracking control for an indoor quadrotor UAV based on the disturbance observer. *Trans. Inst. Meas. Control* **2016**, *38*, 675–692. [[CrossRef](#)]
46. Wang, X.; Sun, S.; van Kampen, E.J.; Chu, Q. Quadrotor fault tolerant incremental sliding mode control driven by sliding mode disturbance observers. *Aerosp. Sci. Technol.* **2019**, *87*, 417–430. [[CrossRef](#)]

47. Liu, X.; Yuan, Z.; Gao, Z.; Zhang, W. Reinforcement Learning-Based Fault-Tolerant Control for Quadrotor UAVs Under Actuator Fault. *IEEE Trans. Ind. Inform.* **2024**, *20*, 13926–13935. [[CrossRef](#)]
48. Chen, F.; Lei, W.; Zhang, K.; Tao, G.; Jiang, B. A novel nonlinear resilient control for a quadrotor UAV via backstepping control and nonlinear disturbance observer. *Nonlinear Dyn.* **2016**, *85*, 1281–1295. [[CrossRef](#)]
49. Pritzl, V.; Vrba, M.; Tortorici, C.; Ashour, R.; Saska, M. Adaptive estimation of UAV altitude in complex indoor environments using degraded and time-delayed measurements with time-varying uncertainties. *Robot. Auton. Syst.* **2023**, *160*, 104315. [[CrossRef](#)]
50. Jeong, H.; Suk, J.; Kim, S. Control of quadrotor UAV using variable disturbance observer-based strategy. *Control Eng. Pract.* **2024**, *150*, 105990. [[CrossRef](#)]
51. Jung, S. Precision Landing of Unmanned Aerial Vehicle under Wind Disturbance Using Derivative Sliding Mode Nonlinear Disturbance Observer-Based Control Method. *Aerospace* **2024**, *11*, 265. [[CrossRef](#)]
52. Hou, Y.; Chen, D.; Yang, S. Adaptive Robust Trajectory Tracking Controller for a Quadrotor UAV with Uncertain Environment Parameters Based on Backstepping Sliding Mode Method. *IEEE Trans. Autom. Sci. Eng.* **2023**, *22*, 4446–4456. [[CrossRef](#)]
53. Izadi, M.; Faiegghi, R. High-gain disturbance observer for robust trajectory tracking of quadrotors. *Control Eng. Pract.* **2024**, *145*, 105854. [[CrossRef](#)]
54. Siddiqui, M.N.; Zhu, X.; Rasool, H.; Afzal, M.B.; Ahmed, N. Model-free low-power observer based robust trajectory tracking control of UAV quadrotor with unknown disturbances. *Aircr. Eng. Aerosp. Technol.* **2024**, *96*, 316–328. [[CrossRef](#)]
55. Gao, Y.; Su, S.; Zong, Y.; Zhang, L. Finite Time Observer-Based Anti-Disturbance Control for Quadrotors Without Velocity Measurements. *IEEE Trans. Aerosp. Electron. Syst.* **2024**, 1–17. [[CrossRef](#)]
56. Kuang, J.; Chen, M. Adaptive Sliding Mode Control for Trajectory Tracking of Quadrotor Unmanned Aerial Vehicles Under Input Saturation and Disturbances. *Drones* **2024**, *8*, 614. [[CrossRef](#)]
57. Mustafa Abro, G.E.; Ali, Z.A.; Zulkifli, S.A.; Asirvadam, V.S. Performance evaluation of different control methods for an underactuated quadrotor unmanned aerial vehicle (QUAV) with position estimator and disturbance observer. *Math. Probl. Eng.* **2021**, *2021*, 8791620. [[CrossRef](#)]
58. Ahmed, N.; Raza, A.; Shah, S.A.A.; Khan, R. Robust composite-disturbance observer based flight control of quadrotor attitude. *J. Intell. Robot. Syst.* **2021**, *103*, 11. [[CrossRef](#)]
59. Thanh, H.L.N.N.; Huynh, T.T.; Vu, M.T.; Mung, N.X.; Phi, N.N.; Hong, S.K.; Vu, T.N.L. Quadcopter UAVs extended states/disturbance observer-based nonlinear robust backstepping control. *Sensors* **2022**, *22*, 5082. [[CrossRef](#)]
60. Li, T.; Zhao, Z.; Ding, S.; Su, J. Composite Controller Design for Quadrotor UAVs with Uncertainties and Noises Based on Combined Kalman Filter and GPIO. *IEEE Trans. Aerosp. Electron. Syst.* **2023**, *60*, 882–892. [[CrossRef](#)]
61. Ju, Y.; Zhang, Y.; Zhu, G. Fuzzy Adaptive Linear Active Disturbance Rejection Control for Quadrotor Load UAV Based on Kalman Filter. *IEEE Access* **2023**, *11*, 104253–104269. [[CrossRef](#)]
62. Mazare, M.; Taghizadeh, M.; Ghaf-Ghanbari, P.; Davoodi, E. Robust fault detection and adaptive fixed-time fault-tolerant control for quadrotor UAVs. *Robot. Auton. Syst.* **2024**, *179*, 104747. [[CrossRef](#)]
63. Kaba, A. Unscented Kalman filter based attitude estimation of a quadrotor. *J. Aeronaut. Space Technol.* **2021**, *14*, 79–88.
64. Patan, M.G.; Caliskan, F. Sensor fault-tolerant control of a quadrotor unmanned aerial vehicle. *Proc. Inst. Mech. Eng. Part G J. Aerosp. Eng.* **2022**, *236*, 417–433. [[CrossRef](#)]
65. Kaba, A.; Kiyak, E. Optimizing a Kalman filter with an evolutionary algorithm for nonlinear quadrotor attitude dynamics. *J. Comput. Sci.* **2020**, *39*, 101051. [[CrossRef](#)]
66. Matisko, P.; Havlena, V. Noise covariances estimation for Kalman filter tuning. *IFAC Proc. Vol.* **2010**, *43*, 31–36. [[CrossRef](#)]
67. Atassi, A.N.; Khalil, H.K. A separation principle for the stabilization of a class of nonlinear systems. *IEEE Trans. Autom. Control* **1999**, *44*, 1672–1687. [[CrossRef](#)]
68. Khalil, H.K.; Praly, L. High-gain observers in nonlinear feedback control. *Int. J. Robust Nonlinear Control* **2014**, *24*, 993–1015. [[CrossRef](#)]
69. Ma, H.J.; Liu, Y.; Li, T.; Yang, G.H. Nonlinear high-gain observer-based diagnosis and compensation for actuator and sensor faults in a quadrotor unmanned aerial vehicle. *IEEE Trans. Ind. Inform.* **2018**, *15*, 550–562. [[CrossRef](#)]
70. Dam, Q.T.; Thabet, R.E.H.; Ali, S.A.; Guerin, F. Observer design for a class of uncertain nonlinear systems with sampled-delayed output using High-Gain Observer and low-pass filter: Application for a quadrotor UAV. *IEEE Trans. Ind. Electron.* **2023**, *71*, 933–942. [[CrossRef](#)]
71. Flores, G.; González-Huitron, V.; Rodríguez-Mata, A. Output feedback control for a quadrotor aircraft using an adaptive high gain observer. *Int. J. Control Autom. Syst.* **2020**, *18*, 1474–1486. [[CrossRef](#)]
72. Jo, A.; Lee, H.; Seo, D.; Yi, K. Model-reference adaptive sliding mode control of longitudinal speed tracking for autonomous vehicles. *Proc. Inst. Mech. Eng. Part D J. Automob. Eng.* **2023**, *237*, 493–515. [[CrossRef](#)]
73. Pham, T.V.; Nguyen, Q.T.T. Model adaptive reference tracking control for uncertain robotic manipulators with input disturbance. *Asian J. Control* **2024**, *26*, 3291–3301. [[CrossRef](#)]

74. Nguyen, N.P.; Hong, S.K. Sliding mode thau observer for actuator fault diagnosis of quadcopter UAVs. *Appl. Sci.* **2018**, *8*, 1893. [[CrossRef](#)]
75. KrstiC, M.; Kanellakopoulos, I.; KokotoviC, P.V. Nonlinear design of adaptive controllers for linear systems. *IEEE Trans. Autom. Control* **1994**, *39*, 738–752. [[CrossRef](#)]
76. Levant, A. Higher-order sliding modes, differentiation and output-feedback control. *Int. J. Control* **2003**, *76*, 924–941. [[CrossRef](#)]
77. Khalil, H.K. *High-Gain Observers in Nonlinear Feedback Control*; SIAM: Philadelphia, PA, USA, 2017. [[CrossRef](#)]

Disclaimer/Publisher’s Note: The statements, opinions and data contained in all publications are solely those of the individual author(s) and contributor(s) and not of MDPI and/or the editor(s). MDPI and/or the editor(s) disclaim responsibility for any injury to people or property resulting from any ideas, methods, instructions or products referred to in the content.